

# Gamma-rays from cascades in close massive binaries containing energetic pulsars

A. Sierpowska & W. Bednarek

*Department of Experimental Physics, University of Łódź, ul. Pomorska 149/153, 90-236 Łódź, Poland*

Accepted Received ; in original form

## ABSTRACT

Some massive binaries should contain energetic pulsars which inject relativistic leptons from their inner magnetospheres and/or pulsar wind regions. If the binary system is compact enough, then these leptons can initiate inverse Compton (IC)  $e^\pm$  pair cascades in the anisotropic radiation field of a massive star.  $\gamma$ -rays can be produced in the IC cascade during its development in a pulsar wind region and above a shock in a massive star wind region where the propagation of leptons is determined by the structure of a magnetic field around the massive star. For a binary system with specific parameters, we calculate phase dependent spectra and fluxes of  $\gamma$ -rays escaping as a function of the inclination angle of the system and for different assumptions on injection conditions of the primary leptons (their initial spectra and location of the shock inside the binary). We conclude that the features of  $\gamma$ -ray emission from such massive binaries containing energetic pulsars should allow to obtain important information on the acceleration of particles by the pulsars, and on interactions of a compact object with the massive star wind. Predicted  $\gamma$ -ray light curves and spectra in the GeV and TeV energy ranges from such binary systems within our Galaxy and Magellanic Clouds should be observed by future AGILE and GLAST satellites and low threshold Cherenkov telescopes such as MAGIC, HESS, VERITAS or CANGAROO III.

**Key words:** gamma-rays: massive binaries – gamma-rays: theory – radiation mechanisms: nonthermal

## 1 INTRODUCTION

It seems obvious that some close massive binary systems should contain young neutron stars able to accelerate leptons and possibly ions to relativistic energies. In fact, numerical simulations of the evolution of neutron stars show that the fraction of systems with not accreting pulsars (during so called ejector phase) may become several percent of the total number of massive binaries (Lipunov 1990). However, due to their proximity to the high density winds of the massive stars most of such systems do not show clear modulation of their radio signal with pulsar rotational period. Therefore, only in the case of broad or highly eccentric binaries the pulsars with periods significantly shorter than 1 second have been discovered (e.g. PSR B1259-63 with the period of 47.8 ms or A0538-66 with the period of 69.2 ms). TeV  $\gamma$ -ray emission, modulated with the period of  $\sim 12.59$  ms, has been also claimed from the compact binary Cyg X-3 (Brazier et al. 1990), but this result has not been confirmed by any other experiment. Other binaries are suspected to contain short period pulsars (e.g. LSI +61 303, Maraschi & Treves 1981), or stellar mass black holes ejecting relativistic

particles highly anisotropically (e.g. Cyg X-1, Bednarek et al. 1990).

In fact, observations of high energy X-ray and  $\gamma$ -ray sources to be coincident with the locations of some binary systems support the hypothesis that the high energy processes play an important role in these sources. For example, EGRET sources have been found in directions towards e.g. LSI +61 303 (2EG J0241+6119, Thompson et al. 1995), Cyg X-3 (2EG J2033-4112, Mori et al. 1997), and LS 5039 (3EG J1824-1514, Paredes et al. 2000). However, no TeV  $\gamma$ -rays from the above mentioned sources have been observed up to now (except early claims during the 80's which were not confirmed by subsequent more sensitive observations; see e.g. Weekes 1992). The limits on TeV emission from PSR B1259-63, recently observed by the CANGAROO group at  $\sim 47$  days and at  $\sim 157$  days after the periastron (Kawachi et al. 2004), are above the theoretical predictions (Kirk et al. 1999, Kawachi et al. 2004, Murata et al. 2003). However, very recently the HESS group reported positive detection of this binary system on the level of 5% of the Crab emission at energies above  $\sim 400$  GeV with the power law spectrum and spectral index -2.8 (Schlenker et al. 2004). The TeV emission has been observed a few days before and after the

periastron passage and declines towards the periastron motion. Observations by the Whipple telescope of other four binary systems containing young pulsars (Hall et al. 2003) have not shown any positive detection of a steady or modulated TeV signal. Another binary system, Cen X-3, reported more recently in the TeV  $\gamma$ -rays (Chadwick et al. 1998, 1999, Atoyan et al. 2002), and also in the GeV  $\gamma$ -rays (Vestrand et al. 1997), contains slowly rotating and accreting neutron star.

In spite of not completely convincing high energy observational results, massive binaries are still often considered as likely sources of  $\gamma$ -rays produced mainly in two general scenarios: (1) the anisotropic injection of particles from neutron stars or black holes, which interact with the radiation or matter inside the binary system (a massive companion, an accretion disk and its corona or a blob, see e.g. Cheng & Ruderman 1991, Aharonian & Atoyan 1991, Levinson & Blandford 1996, Aharonian & Atoyan 1999, Romero et al. 2001, Atoyan et al. 2002, Georganopoulos et al. 2002, Romero et al. 2002, Romero et al. 2003, Bosch-Ramon & Paredes 2004a,b, Orellana & Romero 2004), or (2) the interaction of particles accelerated by a compact object or a shock wave created in collisions of the pulsar and stellar winds (e.g. Vestrand & Eichler 1982, Harding & Gaisser 1990, Tavani et al. 1994, Tavani & Arons 1997, Kirk et al. 1999, Ball & Kirk 2000, Murata et al. 2003) or two stellar winds (e.g. Eichler & Usov 1993, Benaglia & Romero 2003). In fact, the injection of relativistic particles and high energy  $\gamma$ -rays in dense radiation field expected close to the accretion disks around compact objects (Carraminana 1992, Bednarek 1993) and massive companion stars (Protheroe & Stanev 1987, Moskalenko et al. 1993) should result in copious  $\gamma$ -ray production. In very compact binaries and compact objects surrounded by luminous accretion disks, the primary particles can initiate IC  $e^\pm$  pair cascades triggered due to the large optical depths. The  $\gamma$ -ray spectra are then produced with the characteristic cut-offs at a few tens of GeV (Bednarek 1997, Bednarek 2000). It was assumed in the latter works that the secondary  $e^\pm$  pairs produced in the cascade process are isotropised inside the binary system by the random component of the magnetic field.

In the present paper we consider in detail a more specific scenario in which the volume of the binary system is separated by the shock wave into two regions with different properties. The shock appears as a result of collisions of the pulsar and massive star winds. We analyze very compact binary systems which contain a young pulsar and a massive companion star of the OB or WR type able to create soft radiation field in which the optical depths for relativistic leptons are much larger than unity. In fact, young pulsars in binary systems can be responsible for quite different phenomena such as the appearance of jets called microquasars (e.g. Cyg X-3), binary radio pulsars (e.g. PSR 1259-63, SAX J0635+0533) or a long period accreting objects (e.g. A0535+26). It is very difficult to observe some of such systems due to dense stellar winds produced by early type massive stars. However, binaries hidden dense winds should manifest themselves by the presence of large non-thermal luminosities which can, as we argue below, peak in the  $\gamma$ -ray energies. In Sect. 2 we define general conditions inside the massive binary in which the termination shock is created in collisions of the pulsar and stellar winds. The in-

jection of relativistic leptons (electrons or  $e^\pm$  pairs) by the pulsar, their subsequent propagation and interaction with the radiation of the massive star is considered. In Sect. 3 we calculate production of  $\gamma$ -rays in IC  $e^\pm$  cascades initiated by these leptons in the pulsar wind zone (PWZ) by applying the Monte Carlo method. Because of partial absorption of these  $\gamma$ -rays in the massive star wind region (MSWR), the secondary  $e^\pm$  pairs are created and initiate there the second part of the cascade. This cascade differ significantly from the cascade in the PWZ due to the presence of ordered magnetic fields. The spectral and angular features of  $\gamma$ -rays escaping from the PWZ and MSWR are discussed in Sect. 5. As an example we consider the binary system with the parameters derived for the WR star in the Cyg X-3 binary in which there are some observational evidence of the existence of a very young and energetic pulsar with the period of several milliseconds.

## 2 A PULSAR CLOSE TO A MASSIVE STAR

We consider the binary system containing a fast pulsar and a massive companion star ( $M \approx 10M_\odot$ ). It is assumed that the energy loss rate of the pulsar,  $L_{\text{rot}}$ , is high enough that the matter from the massive companion can not accrete onto the pulsar surface neither from the outflow through the Lagrangian point or from the dense stellar wind. This means that the binary system has to be in the ejector phase, in which the structure of the inner pulsar magnetosphere, where efficient acceleration and  $e^\pm$  bfpair creation occur, is not destroyed. The binary systems having the pulsar with the period fulfilling the condition (Harding & Gaisser 1990),

$$P_{\text{ms}} < 31B_{12}^{4/7} \dot{M}_{18}^{-2/7}, \quad (1)$$

should blow away accreting material, where  $P_{\text{ms}}$  is the pulsar period in ms,  $B = 10^{12} B_{12}$  G is its surface magnetic field, and  $\dot{M} = 10^{18} \dot{M}_{18}$  g s $^{-1}$  is the accretion rate.

Let us assume that the pulsar is on a circular orbit around the massive star with the radius  $R_s$ , effective surface temperature  $T_s$ , and surface magnetic field  $B_s$ . The star creates the wind which has the termination velocity  $v_\infty$  and is characterized by the mass loss rate  $\dot{M}$ . The separation of the stars is  $D$ . As a result of the interaction of the pulsar and stellar winds a double shock structure is formed, separated by the contact discontinuity, at the distance determined by the above mentioned parameters of the stars. We apply the simplified model for the structure of the colliding winds based on momentum conservation (Girard & Wilson 1987). In this model the shock structure reaches a steady state configuration under the assumption of negligible pulsar orbital motion. In this case, the shock geometry of specific binary system is determined by the quantity  $\eta$  (Ball & Dodd, 2000), defined as follows:

$$\eta = L_{\text{rot}} / (\dot{M} V_w c), \quad (2)$$

where the wind velocity,  $V_w$ , depends on the radial distance,  $r$ , from the massive star according to (Hamann 1985)

$$V_w(r) = v_\infty (1 - R_A/r)^{1.5}, \quad (3)$$

where  $R_A$  is the Alfvén radius which can be derived by solving the equation  $(1 - R_s/R_A) = \xi (R_s/R_A)^4$ . It has simple

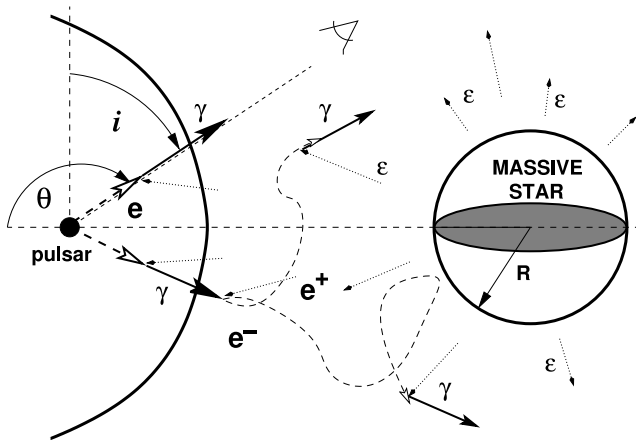


**Figure 1.** The schematic scenario of the interacting neutron star and massive companion inside the compact binary system. Primary leptons, with the Lorentz factors  $\gamma_e$ , are injected by the pulsar and propagate inside the pulsar wind region (PWZ) along direction defined by the angle  $\theta$ , comptonizing soft radiation from the massive star. Secondary  $\gamma$ -rays can be absorbed in the same radiation field either inside the PWZ or, after passing the pulsar wind termination shock, in the massive star wind region (MSWR), triggering an electromagnetic cascade. Leptons propagate radially inside the PWZ but follow the magnetic field structure inside the MSWR.  $\gamma$ -rays from the cascade either escape from the binary system or fall onto the surface of the massive star, depending on the injection parameters of the primary leptons (their energies and directions) and the parameters of the binary system (the massive star parameters and system separation).

approximate solution

$$R_A = R_s \times \begin{cases} 1 + \xi, & \xi \ll 1 \\ \xi^{1/4}, & \xi \gg 1, \end{cases} \quad (4)$$

where  $\xi = B_s^2 R_s / (\dot{M} v_\infty)$ .

The closest radial distance from the pulsar to the termination shock (measured in the plane of the binary system) is then equal to,

$$\rho_0 = D \sqrt{\eta} / (1 + \sqrt{\eta}). \quad (5)$$

In order to estimate  $\rho_0$  we have to solve the set of Eqs. 2–5. Note, that for  $\eta < 1$  the star wind dominates over the pulsar wind and the termination shock wraps around the pulsar. For  $\eta > 1$  the shock wraps around the companion star. For large distances from the massive star the shock tends asymptotically to a cone characterized by a half-opening angle  $\psi$ ,

$$\psi = 2.1(1 - \eta^{-2/5}/4)\eta^{-1/3}. \quad (6)$$

We approximate the structure of the termination shock by the sphere of radius  $\rho_0$  for  $\theta > \theta_0$  ( $\theta$  is defined in Fig. 1), and by a cone for  $0 < \theta < \theta_0$ , where the angle  $\theta_0$  is defined as  $\theta$  and is given by the perpendicular line from pulsar to the generator of the cone. The shock is unterminated for  $\theta < \psi$ .

It is assumed in these simple estimations that the pulsar and stellar winds are symmetric. In a more realistic case the dependence of the wind pressure on the distance from the equatorial plane of both stars should be taken into account. This might result in more complicated structure of the shock surface and involve more parameters which would prevent clear analysis of the angular features of high energy  $\gamma$ -ray

emission from such compact binaries. In a future work (Sierpowska & Bednarek 2004a), in which we apply such a model to the  $\gamma$ -ray production in the binary pulsar PSR 1259-63 on the orbit around the Be star, the effects associated with the non-spherical stellar wind will be taken into account.

In order to perform detailed calculations in the case of specific binary we apply as an example the parameters expected for the massive WR star in the Cyg X-3 system. This is a short period compact binary,  $\tau = 4.8$  hr, with the massive star radius  $< 3 - 6R_\odot$ , surface temperature  $T_s > (7 - 9) \times 10^4$  K, separation of the components  $3.2 < D/R_\odot < 5.6$ , and the mass loss rate  $\dot{M} \sim 1.1 \times 10^{-5} M_\odot \text{ yr}^{-1}$  (Cherepashchuk & Moffat 1994). The orbital, phased resolved infrared spectra in the outburst and quiescent stages are consistent with the high orbital inclination of the system with respect to the observer at the Earth,  $i > 60^\circ$ , provided that the mass of the massive star is in the range,  $5 < M_{WR}/M_\odot < 11$  (Hanson et al. 2000). The infrared observations by van Kerkwijk et al. (2002) are consistent with the high orbital inclination,  $i = 74^\circ$ , and the mass loss rate in the range  $\dot{M} \sim 1.2 \times 10^{-4} M_\odot \text{ yr}^{-1}$  (based on the infrared data) and  $\dot{M} \sim 0.6 \times 10^{-5} M_\odot \text{ yr}^{-1}$  (based on the increase of orbital period). The stellar wind has terminal velocity  $V_\infty = 1.45 \times 10^3 \text{ km s}^{-1}$ . On the other hand, the inclination angle of system derived from the X-ray Chandra data is much lower,  $i \approx 24^\circ$ . The mass of the compact object has been constrained by  $< 3.6M_\odot$ , and the mass and radius of the stellar companion by  $< 7.3M_\odot$  and  $R_s < 1.6R_\odot$  (Stark & Saia 2003).

Based on the above observational constraints, we adopt the following parameters for our specific binary system. A Wolf-Rayet type star with a radius  $R_s = 1.6 \times R_\odot$ , an effective temperature,  $T_{\text{eff}} = 1.36 \times 10^5$  K, and a typical surface magnetic field,  $B_s \sim 10^2 - 10^3$  G (Usov & Melrose). The mass loss rate is  $\dot{M} \sim 0.8 - 8.0 \times 10^{-5} M_\odot \text{ yr}^{-1}$ , the velocity of the stellar wind at infinity  $v_\infty \sim (1 - 5) \times 10^8 \text{ cm s}^{-1}$ , and the star rotational velocity  $v_{\text{rot}} \sim (0.1 - 0.2)v_\infty$ . The pulsar has a period  $P_{\text{ms}} = 12.59$  and a surface magnetic field  $B_s = 4.95 \times 10^{11}$  G (Brazier et al. 1990). It is on a circular orbit, with a separation of  $D = (3.6 \pm 1.2)R_\odot = 2.25 \times R_s$  (Stark & Saia 2003). For these parameters, the pulsar energy loss rate is,

$$L_{\text{rot}} \approx 6 \times 10^{43} B_{12}^2 P_{\text{ms}}^{-4} \text{ erg s}^{-1} \approx 6 \times 10^{38} \text{ erg s}^{-1}. \quad (7)$$

For the above mentioned parameters of the massive companion in the Cyg X-3, the value of the parameter  $\eta$  (see Eq. 2) is in the range  $0.067 < \eta < 0.67$  (for fixed  $V_\infty = 1.45 \times 10^3 \text{ km s}^{-1}$ ). For further calculations we apply the average value  $\eta = 0.3$  and for comparison the lowest value  $\eta = 0.06$ .

The conditions in the two regions of the binary system, i.e the PWZ and the MSWR, separated by the shock structure differ significantly. Below the shock, inside the PWZ, relativistic leptons are frozen in the magnetized pulsar wind which propagate radially from the pulsar. Therefore, their synchrotron losses are neglected in our cascade calculations. We consider the IC cascade in the PWZ assuming that the thermal radiation from the massive star dominates in the main volume of this region, neglecting the other sources of soft photons e.g. such as the thermal emission from the neutron star surface or the nonthermal emission from the inner pulsar magnetosphere. This is true if the temperature of the whole neutron star surface is below  $T_{\text{NS}} \sim 6 \times 10^6$  K.

But such surface temperature is characteristic for the cooling neutron star in the age of only a few months after formation (Nomoto & Tsuruta 1987). This limit temperature has been obtained by comparing the energy density of thermal radiation from the massive star,  $U_s \approx \sigma_{SB} T_s^4 (R_s/D)^2$ , where  $\sigma_{SB}$  is the Stefan-Boltzman constant, with the energy density of thermal radiation from the neutron star,  $U_{NS} \approx \sigma_{SB} T_{NS}^4 (R_{NS}/R_{LC})^2 (1 + \cos \theta)$ , at the distance of the light cylinder radius,  $R_{LC}$ . For the period of the pulsar as suggested in the Cyg X-3 binary,  $P = 12.59$  ms, we obtain  $R_{NS}/R_{LC} \approx 60$ . The approximate angle of interaction between leptons and photons coming from the neutron star surface is then  $\theta = \pi - R_{NS}/R_{LC}$  radians, assuming the case of a spherical wind. The estimate of the possible contribution of the nonthermal radiation from the pulsar inner magnetosphere is very difficult since the geometry of this nonthermal emission is not well known. We comment that this nonthermal photons has to be strongly collimated along the direction of motion of relativistic leptons as postulated by the observation of very narrow peaks in the light curves of young pulsars. Therefore, its importance should be strongly suppressed. However, Bogovalov & Aharonian (2000) calculated possible  $\gamma$ -ray emission from the vicinity of the light cylinder in the case of the Crab pulsar applying a specific model for the radiation close to the light cylinder radius. According to these calculations the optical depth for leptons in the thermal radiation field of the Crab pulsar is very low at the light cylinder. However, in the nonthermal radiation from the pulsar inner magnetosphere, the optical depth for leptons can be significant at the distance up to a few light cylinder radii. We conclude that the soft radiation in the main part of the PWZ is dominated by the thermal radiation from the massive star. Although, the important contribution of the nonthermal radiation from the inner pulsar magnetosphere at distances just above the light cylinder radius can not be excluded. This problem should be studied in a more detail when reliable models of the high-energy processes in the pulsar magnetospheres are better constrained.

Leptons which move through the PWZ interact efficiently with the soft radiation of the massive companion initiating IC  $e^\pm$  pair cascade. The charged products of this cascade arrive finally to the shock region in the pulsar wind and follow the flow along the shock surface. The power in these secondary leptons is relatively low with respect to the power in secondary cascade  $\gamma$ -rays in the case of very close binary systems considered in this paper. The secondary  $\gamma$ -rays move into the massive star wind region. Some of them escape the binary system but a significant part can be converted into the next generation of  $e^\pm$  pairs which have to follow the complex structure of the magnetic field present in the stellar wind. These pairs can trigger further cascading processes producing next generation of  $\gamma$ -rays at directions which depend not only on the injection geometry of primary leptons but also on the geometry of the magnetic field. All these processes are discussed in detail in this paper and the spectra of  $\gamma$ -rays escaping at different angles with respect to the plane of the system and as a function of the phase of the pulsar on its orbit around the massive star are calculated.

## 2.1 Injection of leptons by the pulsar

Young pulsars are efficient sources of energetic leptons, i.e. electrons and positrons. These leptons originate in the cascade processes occurring in the inner pulsar magnetosphere, as expected in terms of the polar cap model (e.g. Ruderman & Sutherland 1975, Arons & Sharlemann 1979, Daugherty & Harding 1982) and the outer gap model (e.g. Cheng et al. 1986). Leptons escape through the pulsar light cylinder to the pulsar wind zone (PWZ) where they can be additionally accelerated either just above  $R_{LC}$  (e.g. Beskin & Rafikov 2000) or linearly through the PWZ (e.g. Contopoulos & Kazanas 2002), or at the pulsar wind shock (e.g. Kenne & Coronity 1984).

In this paper we consider two models for the primary spectra of leptons injected into the radiation field of the massive star:

(i) The power law spectrum of injected leptons between 100 MeV and 500 GeV and the spectral index -1.2, as envisaged in the recent calculations of the spectra of leptons escaping from the inner magnetosphere performed by Hibschman & Arons (2001).

(ii) The monoenergetic injection of leptons with energies  $10^6$  MeV corresponding to the Lorentz factors of the pulsar wind with the parameters typical for the Crab pulsar. These leptons have very similar energies to those ones expected for the supposed pulsar in Cyg X-3 binary system due to the similar value of  $B/P^2$ , which determine the maximum potential drops through the pulsar magnetosphere. In fact, adopting the formulas of the slot-gap pair-cascade model (Arons 1983) for a  $e^\pm$  pair generation rate,  $N_{e^\pm}$ , and small ratio  $\sigma_{pw}$  of Poynting flux to kinetic energy flux in the wind not far from the light cylinder radius, the Lorentz factor  $\gamma_{pw}$  of the pulsar wind can be estimated from (Melatos et al. 1995),

$$\gamma_{pw} = L_{rot}/(1 + \sigma_{pw}) N_{e^\pm} m_{e^\pm} c^2, \quad (8)$$

where  $m_{e^\pm}$  is the electron mass, and  $c$  is the velocity of light. For the considered here parameters of the pulsar  $N_{e^\pm} \approx 2.8 \times 10^{37} s^{-1}$  and the pulsar wind Lorentz factor can be as high as  $\gamma_{pw} \sim 10^7$  (Melatos et al. 1995). The small ratio  $\sigma_{pw}$  can be obtained in the narrow boundary layer near the light cylinder as suggested by Beskin & Rafikov (2000). These authors argue that the energy of the magnetized wind may be transferred to leptons with the Lorentz factors  $\sim 10^6$ .

Most of the calculations presented below are shown for the power in injected spectrum of leptons normalized to  $10^6$  MeV  $sr^{-1}$  in order to allow direct comparison between the cases of power law and monoenergetic injection of leptons. The absolute fluxes of  $\gamma$ -rays produced in the cascade can be then obtained by multiplying by the factor  $\sim 3 \times 10^{37} s^{-1}$  which is calculated from normalization of the power equal to  $10^6$  MeV to the total rotational energy lost by the pulsar (see Eq. 8).

## 2.2 Conditions for propagation of leptons and gamma-rays

We are interested in binary systems in which relativistic leptons, injected by the pulsar, can develop the IC  $e^\pm$  pair

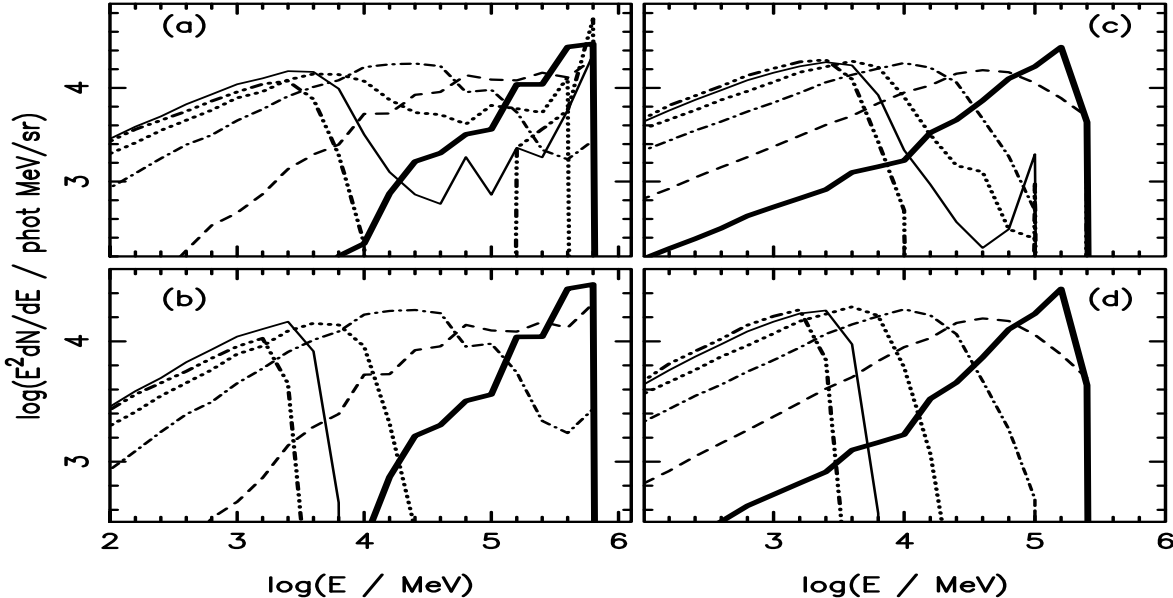


**Figure 3.** The  $\gamma$ -ray spectra produced in the cascade inside the PWZ in the case of injection of primary leptons with: the monoenergetic spectrum and energy  $10^6$  MeV (on the left), and the power law spectrum (on the right). The spectra are shown for different injection angles of the primary leptons:  $\theta = 0^\circ$  (thick solid curve),  $30^\circ$  (dashed),  $60^\circ$  (dot-dashed),  $90^\circ$  (dotted),  $120^\circ$  (thin solid), and  $150^\circ$  (dot-dot-dot-dashed). The  $\gamma$ -ray spectra which arrive to the shock region (defined by  $\eta = 0.3$ ) are shown in (a) and (c), and the  $\gamma$ -ray spectra escaping to the observer at the infinity (after their absorption inside the MSWR) are shown in (b) and (d). The spectra are obtained by sorting photons within the intervals with the width  $\Delta(\log E) = 0.2$  with the lower boundary of the interval marked in the figures.

cascades in the anisotropic radiation of the massive companion. Considered by us binary system meets this requirement if the optical depths for IC scattering of massive star thermal radiation and for  $\gamma$ -rays absorption process in the same radiation are much larger than unity. For the injection place of leptons and  $\gamma$ -rays equal to the separation distance between the pulsar and the WR star,  $D = 2.25R_s$ , and other parameters as mentioned above, we calculate the optical depths up to the infinity for different angles of injection measured with respect to the direction defined by the centres of these stars and as a function of lepton energies (see Fig. 2). The optical depths for leptons are very large in considered energy range. Moreover,  $\gamma$ -rays with energies above a few GeV have high probability of interaction for all directions (optical depth larger than unity). Therefore, leptons injected with energies large enough should develop IC  $e^\pm$  pair cascade.

In fact, the cascade can start to develop already inside the PWZ (see Fig. 2b). The optical depths for all injection angles, calculated up to the location of the shock defined by  $\eta = 0.3$ , are much larger than unity at specific energy ranges. In Fig. 2c the dependence of the optical depths for leptons and  $\gamma$ -rays on the location of the shock inside the binary system is shown. It is clear that even for the extreme values of  $\eta = 0.06$  and  $0.6$  leptons should develop efficient cascades if injected with energies above  $\sim 10$  GeV. From comparison of Figs. 2a and 2bc we find that the optical depths for  $\gamma$ -ray photons which are produced below the shock (in the PWZ) but propagate through the MSWR are still much larger than unity. Therefore, these  $\gamma$ -rays partially convert into the next generation of  $e^\pm$  pairs in the MSWR. These  $e^\pm$  pairs produce next generation of  $\gamma$ -rays which angular distribution on the sky may differ from initial injection directions of primary

leptons due to the presence of a complex magnetic field in the MSWR. For that reason we consider the cascades developing inside the PWZ and MSWR separately.

### 3 PULSAR WIND REGION

It is assumed that energetic leptons are injected from the vicinity of the pulsar light cylinder and propagate radially from the pulsar almost at rest with respect to the pulsar wind. In this case we neglect the synchrotron losses of leptons during their propagation up to the pulsar wind shock. If the optical depths are such as shown in Figs. 1, leptons develop IC  $e^\pm$  pair cascade whose efficiency depends on the injection parameters of these primary particles (initial energies of leptons, their injection directions and parameters of the binary system and massive star). We assume that the cascade initiated by specific primary lepton in the PWZ develops in one dimension, i.e. in the direction of propagation of the primary particle. Such one-dimensional cascade develops up to the pulsar wind shock. The secondary  $\gamma$ -rays pass through the shock into the massive star wind region where they can be additionally absorbed producing next generation of energetic  $e^\pm$  pairs. For considered large optical depths, only the  $\gamma$ -rays with energies below the threshold for  $e^\pm$  pair production escape freely from the binary system. The secondary  $e^\pm$  pairs which are produced in the PWZ are captured by the magnetic field of the shock region and move along its surface with the pulsar wind plasma. However, in the case of compact binary systems such as Cyg X-3, we can neglect the contribution of secondary  $e^\pm$  pairs to the total escaping  $\gamma$ -ray spectrum, because the part of energy of the primary leptons transferred to the secondary  $e^\pm$  pairs is rela-

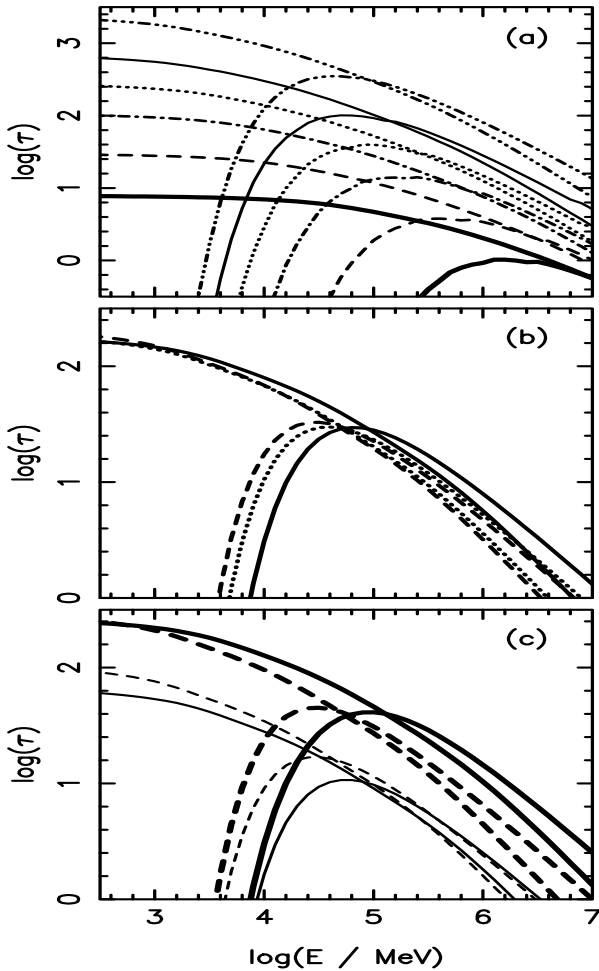


**Figure 2.** The optical depths for leptons on ICS process, and for  $\gamma$ -rays on  $e^\pm$  pair production in the anisotropic radiation of the massive star during their rectilinear propagation from the injection place at the distance  $D = 2.25R_s$  from the massive star up to the infinity (figure (a)). The optical depths are shown as a function of particle energies for the case of injection at the angle  $\theta$ , measured from direction defined by the centers of these stars (see Fig. 1):  $0^\circ$  (thick full curves),  $30^\circ$  (dashed),  $60^\circ$  (dot-dashed),  $90^\circ$  (dotted),  $120^\circ$  (thin full), and  $150^\circ$  (dot-dot-dot-dashed). (b) As in (a) but for particles propagating only to the termination shock defined by  $\eta = 0.3$  and for the injection angles  $90^\circ$  (solid lines),  $120^\circ$  (dotted lines) and  $150^\circ$  (dashed lines). Note that for the angles  $0^\circ - 60^\circ$ , the optical depths are the same as in (a) due to the lack of boundary on the rectilinear propagation caused by the presence of the shock. (c) As in (b) but for two specific locations of the shock defined by  $\eta = 0.06$  and  $0.6$  and for the injection angles of primary leptons equal to  $90^\circ$  (solid lines) and  $150^\circ$  (dashed lines).

tively low compared to that one transferred to the secondary  $\gamma$ -rays, as we show later. The influence of this part of leptonic cascade on the total  $\gamma$ -ray spectrum escaping from the system will be considered in the future work dedicated to wider binary systems.

### 3.1 Gamma-ray spectra from the PWZ

We follow the development of such IC  $e^\pm$  pair cascade in the anisotropic radiation of the massive star assuming that

the primary particles are injected in the place corresponding to the location of the pulsar in the binary system (the light cylinder radius can be safely neglected with respect to the characteristic dimension of the PWZ). The procedure for the cascade Monte Carlo simulations in the PWZ is generally the same as used in Bednarek (1997, 2000) except for the assumption on the local isotropisation of secondary  $e^\pm$  pairs applied in that paper. In this paper it is assumed that the secondary cascade  $e^\pm$  pairs follow the direction of the parent  $\gamma$ -rays. The distance of the first interaction of a lepton in the IC scattering process,  $L_{\text{IC}}$ , is determined by sampling from the optical depth calculated for specific parameters of lepton injection place.  $L_{\text{IC}}$  is found for the random number  $P_1$  applying the formula,

$$P_1 = \exp \left( - \int_0^{L_{\text{IC}}} \lambda_{\text{IC}}^{-1}(E, L, \theta) dL \right), \quad (9)$$

where  $\lambda_{\text{IC}}(E, L, \theta)$  is the mean free path for IC scattering of lepton with energy  $E$ , at the place defined by the propagation distance  $L$  and the angle  $\theta$  (see Fig. 1).  $\lambda_{\text{IC}}$  is calculated from the formula

$$\lambda_{\text{IC}}^{-1}(E, L, \theta) = \int d\mu (1 + \mu) \int d\phi \int N(\varepsilon, \Omega) \sigma_{\text{KN}} d\varepsilon, \quad (10)$$

where  $\mu = \cos \theta$  is the cosine of the angle between lepton and the incident soft photon,  $N(\varepsilon, \Omega)$  is the differential density of soft photons, and  $\sigma_{\text{KN}}$  is the Klein-Nishina cross section. The limits of integrations in this formula are constrained by the geometry of the scattering process (propagation directions of leptons and thermal photons from the massive star) and the kinematics of the IC process. Since these limits are very complicated (several cases have to be considered), they will be published separately in Sierpowska (2004). The distance at which secondary  $e^\pm$  pair is produced in collisions of the  $\gamma$ -ray photon with the soft photon is obtained in a similar way (see Eqs. 9 and 10) by replacing the Klein-Nishina cross section by the cross section for  $e^\pm$  pair production in the two photon collision (see Appendix A in Bednarek 1997). The subsequent places of the interaction of secondary leptons and  $\gamma$ -rays are determined in the same way by replacing the lower limit in the integral in Eq. (9) from the  $n$ -th cascade step by the upper limit in the integral from the previous,  $(n-1)$ -th cascade step. The neutron star is relatively close to the massive star with respect to its dimensions as the separation of the components is only 2.25 larger than the radius of the massive star. Therefore, the geometrical effects connected with limited solid angle of impinging soft photons have to be taken into account when considering the IC scattering process.

The energies of secondary particles produced by parent leptons or  $\gamma$ -rays as a result of the interaction with the soft photons from the massive star are obtained for the random number  $P_2$  by sampling from the differential energy distributions of these secondary particles according to the relation

$$P_2 = \left( \int_0^{E_{\text{sec}}} N dE \right) \left( \int_0^{E_{\text{sec},m}} N dE \right)^{-1}, \quad (11)$$

where  $N$  is the differential spectrum of secondary particles

$\eta = 0.3$			$\eta = 0.06$	
$\theta$	shock [%]	esc [%]	shock [%]	esc [%]
(a)	0	-	58	-
	30	-	70	70
	60	-	88	19
	90	84	53	10
	120	82	47	12
	150	83	31	14
	180	80	-	44
(b)	0	-	59	62
	30	-	82	83
	60	-	94	84
	90	92	87	48
	120	90	74	52
	150	87	64	56
	180	87	-	85

**Table 1.** The percentage of primary leptons initial energy with monoenergetic (a) and power law spectra (b) (see text for details) which is transferred to the  $\gamma$ -rays in the cascade process for two locations of the shock defined by  $\eta = 0.3$  and 0.06. The part of energy in  $\gamma$ -rays which reached the shock region is marked by *shock* and which managed to escape to the infinity is marked by *esc*. For small angles  $\theta$  the shock is not present, and for  $\theta = 180^\circ$   $\gamma$ -rays do not escape but collide with the surface of the massive star.

( $e^\pm$  pairs or  $\gamma$ -rays), produced by the parent particle with energy  $E$  ( $\gamma$ -ray or lepton, respectively), calculated at a specific location inside the PWZ which is defined by  $L_{IC}$  for the IC process and by  $L_{\gamma-\gamma}$  for  $\gamma$ -ray absorption process (see for details the Appendix B and C in Bednarek 1997);  $E_{sec,m}$  is the maximum energy of produced secondary particle allowed by the kinematics of specific process, i.e. IC scattering or  $\gamma-\gamma$  absorption;  $E_{sec}$  is the simulated energy of produced secondary particle. The energy of parent lepton after  $n$ -th interaction and the energy of secondary leptons, produced in  $\gamma-\gamma$  absorption, is found by applying energy conservation, i.e.  $E_{e^\pm,n} = E_{e^\pm,n-1} - E_{\gamma,n}$  and  $E_{\gamma,n-1} = E_{e^+,n} + E_{e^-,n}$ . Since we are interested in high energy  $\gamma$ -rays, i.e.  $> 100\text{ MeV}$ , the cascading procedure is switched off when the secondary leptons are cooled to energies below 500 MeV. Such leptons are not able to produce  $\gamma$ -rays above 100 MeV in the radiation described by the black body spectrum with temperature  $\sim 10^5\text{ K}$ , typical for the massive stars considered by us. The simulation procedure of the  $\gamma$ -ray photon interaction place and the energies of secondary leptons from photon absorption is analogous to what was described above.

The cascade processes occurring inside the PWZ are axially symmetric with respect to the direction defined by the centers of stars. Therefore, the spectra of  $\gamma$ -rays, these at the location of the shock front and those ones escaping to the infinity through the radiation of the MSWR, are calculated only as a function of the injection angle  $\theta$ . The  $\gamma$ -ray spectra have been obtained for two, mentioned in Sect. 2.2, distributions of primary leptons and the location of the shock defined by  $\eta = 0.3$  (see Figs. 3 for the monoenergetic and the power law spectra of primary leptons). Note that photons are sorted within the intervals with the width

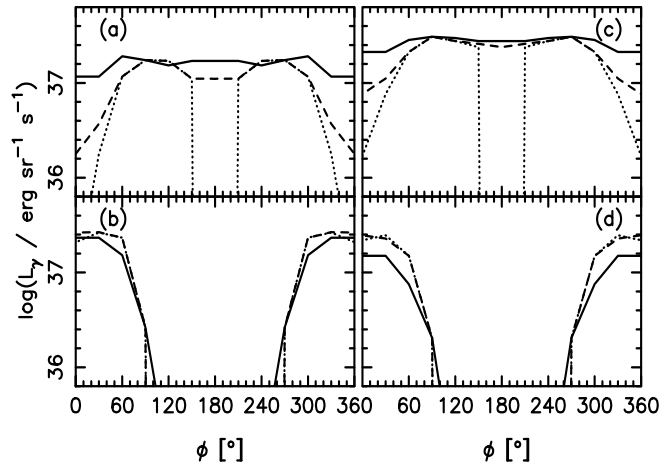


**Figure 4.** The  $\gamma$ -ray light curves in two energy ranges,  $0.1 - 10\text{ GeV}$  ((a) and (c)) and  $10 - 10^3\text{ GeV}$  ((b) and (d)), produced in the cascade process occurring inside the PWZ. The cascade is initiated by leptons with the monoenergetic (figures on the left) and the power law spectra (on the right) for selected values of the inclination angles  $i = 30^\circ$  (solid curve),  $60^\circ$  (dashed), and  $90^\circ$  (dotted) measured from the normal to the plane of the binary system.

$\Delta(\log E) = 0.2$ . The basic features of the  $\gamma$ -ray spectra observed at infinity, i.e. after their partial absorption in the radiation field of the MSWR, can be easily understood if analyzed in the context of the optical depths shown in Figs. 1ab. Only primary leptons propagating in the outward direction (with respect to the massive star) can produce  $\gamma$ -ray fluxes above  $\sim 100\text{ GeV}$ , being potentially detectable by telescopes operating at very high energies (VHE) (Figs. 3bd). On the other hand, the  $\gamma$ -ray spectra escaping in the inward directions, i.e. close to the limb of the massive star, have comparable intensities at energies below  $10\text{ GeV}$  (HE range) within a factor of 2-3. Moreover, these spectra show cut-offs close to  $\sim 10\text{ GeV}$  which are determined by the surface temperature of the massive star. Therefore, the anticorrelation between the  $\gamma$ -ray emission in the HE and VHE ranges is expected from such compact luminous binaries. The spectra of  $\gamma$ -rays produced in the PWZ and arriving to the shock region are shown in Figs. 3ac. The difference between  $\gamma$ -ray spectra shown in Figs. 3ac and 3bd gives us the information about the importance of absorption processes in the MSWR. It is evident that the high energy part of the  $\gamma$ -ray spectrum produced in the PWZ is strongly absorbed during propagation through the MSWR if the primary leptons are injected in the hemisphere containing the massive star, i.e. for the angles  $\theta > 90^\circ$ . Important information on the efficiency of  $\gamma$ -ray production can be derived from analysis of the percentage of the energy of primary leptons which is converted in the PWZ cascade process into the  $\gamma$ -ray photons. Table 1 reports these efficiencies at the infinity (marked by *esc*) and at the location of the shock inside the binary system (marked by *shock*) defined by  $\eta = 0.3$  and 0.06. Most of the initial lepton energy can be converted into the  $\gamma$ -rays in such a cascade already at the distance of the shock in the case of dense soft radiation field of such compact massive companion.

A significant part of the power of produced  $\gamma$ -ray for the directions of primary leptons towards the massive star

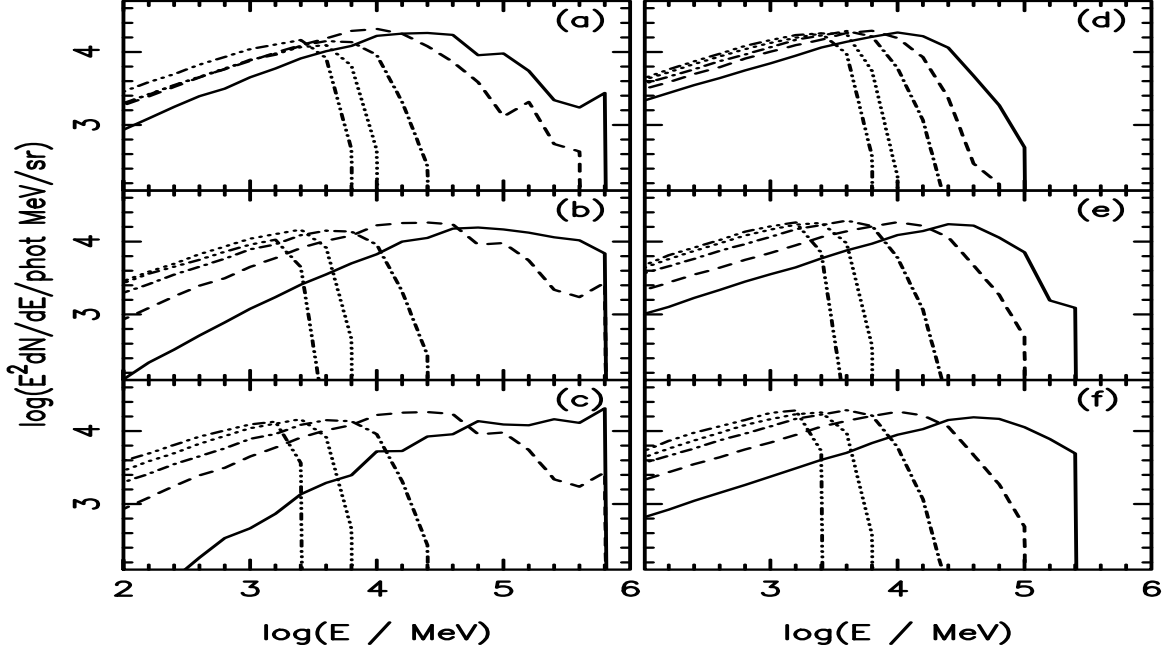


**Figure 5.** The  $\gamma$ -ray spectra escaping from the binary system for different phases of the pulsar on its orbit around the massive star (measured with respect to the location of the observer),  $\varphi = 30^\circ$  (solid curve)  $60^\circ$  (dashed),  $90^\circ$  (dot-dashed),  $120^\circ$  (dotted),  $180^\circ$  (dot-dot-dot-dashed), and different inclination angles of the binary system  $i = 30^\circ$  ((a) and (d)),  $60^\circ$  ((b) and (e)), and  $90^\circ$  ((c) and (f)).  $\gamma$ -rays are produced in the PWZ cascade by primary leptons with the monoenergetic (figures on the left) and the power law spectrum (on the right).

( $\theta > 90^\circ$ ) can be again converted into the next generation of  $e^\pm$  pairs in the absorption process in the MSWR (see the difference between *shock* and *esc* in Table 1). Therefore, possible contribution of the cascades initiated by these secondary  $e^\pm$  pairs in the MSWR to the total  $\gamma$ -ray spectrum escaping from the binary system can not be neglected. These secondary  $e^\pm$  pairs propagate in the MSWR along the paths which are determined by the structure of the magnetic field in the wind of the massive star. That is why, the next generation of  $\gamma$ -rays produced by them move in directions which can completely differ from the initial angular distribution of  $\gamma$ -rays escaping from the PWZ. This more complicated cascade with the re-distribution of charged particles with respect to their initial directions is discussed in details in the next section.

### 3.2 Gamma-ray light curves and phase resolved spectra

In order to investigate in more details the angular dependence of the  $\gamma$ -ray emission produced in the cascade inside the PWZ, we calculate the  $\gamma$ -ray light curves which should be observed at different inclination angles of the binary system. The results are shown for the two, HE and VHE, energy ranges (i.e.  $0.1 - 10$  GeV and  $10 - 10^3$  GeV) in the case of primary leptons injected into the PWZ with the monoenergetic and power law distributions (see Figs. 4). The  $\gamma$ -ray luminosities are calculated after normalization of the power in primary leptons to the rotational energy lost by the pulsar,  $L_e = L_{\text{rot}}$ . Clear anticorrelation in the  $\gamma$ -ray curves is observed between these two energy ranges for both initial spectra of primary leptons. The VHE emission is mainly limited to the phases when the pulsar is in front of the massive star

( $\varphi = 0^\circ$ ). In contrast, the HE emission is much more uniform with significant decrease at phases around  $0^\circ$  at which the VHE emission is the strongest. The disappearance of  $\gamma$ -ray emission for large inclination angles of  $i > 90^\circ - \alpha$  (where  $\alpha = 26.4^\circ$  is the angular extend of the massive companion observed from the distance of the binary separation) and at the phase close to  $180^\circ$ , is connected with the total eclipse of the pulsar by the massive companion. The  $\gamma$ -ray spectra for selected phases of the pulsar on its orbit and the inclination angles mentioned in Figs. 4 are shown in Figs. 5. The  $\gamma$ -ray spectral shapes do not differ significantly below a few GeV (spectral index close to -1.5) for half of the pulsar phases, independently on the inclination angle of the binary system. The level of this emission vary only by a factor of 2-3. In contrast, the VHE emission is limited to a relatively small range of phases with clear dependence on the inclination angle of the binary.

## 4 MASSIVE STAR WIND REGION

As we have shown above, a significant part of  $\gamma$ -rays from the PWZ which passed the termination shock is effectively absorbed in the MSWR by dense radiation field of the massive star (see Table 1). However, the next generation of  $e^\pm$  pairs is forced to follow the local magnetic field lines and their directions of propagation can change significantly with respect to the directions of their parent  $\gamma$ -rays. Therefore, the development of the cascade in the MSWR becomes much more complicated, determined by the complex magnetic field structure and the cascade is not further one-dimensional. The next generation  $\gamma$ -rays are usually produced at com-

pletely different angles than the initial directions of the PWZ cascade  $\gamma$ -rays.

It is assumed in these cascade calculations that synchrotron energy losses of the cascading  $e^\pm$  pairs can be neglected with respect to their energy losses on the ICS. In fact, the comparison of energy densities of the magnetic field  $\sim 2.5 \times 10^{16}$  eV cm $^{-3}$ , for the surface magnetic field of the star  $B_s = 10^3$  G, and the thermal radiation  $\sim 8.5 \times 10^{17}$  eV cm $^{-3}$ , for the temperature of the star  $T_s = 1.36 \times 10^5$  K, show that the IC losses should clearly dominate over the synchrotron process. Further from the star the energy density of radiation drops with the square of the distance and the energy density of magnetic field drops with the forth power of the distance (see Eq. (17), note that the Alfvén radius is very close to the stellar surface for the considered here parameters). Therefore, if the IC losses dominate at the stellar surface it have to dominate everywhere above the star. It has been shown in Bednarek (1997, see Eq. 4 in that paper) that the Bremsstrahlung energy losses of leptons in the wind of the massive star are negligible with respect to their IC losses in the Thompson (T) regime for the parameters of the wind and the star considered here and the Lorentz factors of leptons above the limiting the value  $10^3$  considered in the cascade process. However in the present paper we also consider leptons with energies up to  $10^6$  MeV. It is necessary to discuss in a more detail the case of the IC losses in the Klein-Nishina (KN) regime. The IC losses of leptons with the Lorentz factors  $\gamma$  in the T regime and the thermal radiation with temperature  $T_s$  can be approximated by

$$\left(\frac{dE}{dt}\right) \approx 1.3 \times 10^{-22} \gamma^2 T_s^4 \text{ MeV s}^{-1}. \quad (12)$$

We can estimate energy losses in the KN regime by putting into the above formula the Lorentz factor of leptons between the KN and T regimes, i.e.  $\gamma \approx 2 \times 10^4$  for  $T_s = 10^5$  K. Then we get

$$\left(\frac{dE}{dt}\right)_{\text{KN}} \approx 5 \times 10^6 \text{ MeV s}^{-1}. \quad (13)$$

Note that the logarithmic dependence of energy losses in the KN regime has been neglected. On the other hand, the bremsstrahlung energy losses can be approximated by

$$\left(\frac{dE}{dt}\right)_{\text{brem}} \approx 1.4 \times 10^{-16} N E \text{ MeV s}^{-1} \quad (14)$$

where  $N$  is the density of particles in cm $^{-3}$  and  $E$  is energy of leptons in MeV. For the extreme energies of injected leptons considered in the cascade process ( $E = 10^6$  MeV), we obtain

$$\left(\frac{dE}{dt}\right)_{\text{brem}} \approx 1.4 \times 10^{-10} N \text{ MeV s}^{-1} \quad (15)$$

From the comparison of  $(dE/dt)_{\text{KN}}$  with  $(dE/dt)_{\text{brem}}$ , we obtain the critical density of the matter  $N_{\text{cr}} \approx 4 \times 10^{16}$  cm $^{-3}$ .

Let's estimate a typical density of the massive star wind in the MSWR close to the stellar surface,

$$N_w = \dot{M}/4\pi R_s^2 V_w, \quad (16)$$

which for the wind velocity  $V_w = 10^8$  cm s $^{-1}$  and the

mass loss rate  $\dot{M} = 4 \times 10^{-5} M_\odot$  yr $^{-1}$ , gives  $\sim 8 \times 10^{13}$  cm $^{-3}$ . So then, density of the massive star wind is 2-3 orders of magnitude lower than the critical density,  $N_{\text{cr}}$ , above which the Bremsstrahlung energy losses dominate over the IC losses in the KN regime. Therefore, we conclude that the Bremsstrahlung process can be safely neglected with respect to the IC process for the model considered in this paper.

Below we describe the procedure applied for the calculation of the cascade processes with the presence of the magnetic field in the MSWR.

#### 4.1 Magnetic field structure inside MSWR

The magnetic field in the wind of the massive star can have complicated structure. In the region very close to the massive star surface it is characterized by dipolar component. At a certain distance, the radial component starts to dominate due to the presence of the ionized plasma, and at larger distances the magnetic field becomes toroidal due to the rotation of the massive star. The strength of the magnetic field as a function of distance from the center of the massive star can be described by the following equations (Usov & Melrose, 1992),

$$B(r) \approx B_s \times \begin{cases} (R_s/r)^3, & R_s \leq r < R_A, \\ R_s^3/(R_A r^2), & R_A < r < R_{\text{tor}}, \\ (v_{\text{rot}}/v_\infty) (R_s^2/(R_A r)), & R_{\text{tor}} < r, \end{cases} \quad (17)$$

where  $R_{\text{tor}}$  is the radius of the toroidal field defined by the rotation velocity of the massive star  $v_{\text{rot}}$  and the star wind velocity at the infinity  $v_\infty$ ,  $R_{\text{tor}} = R_s v_\infty / v_{\text{rot}}$ . In the case of the typical parameters of considered here for the WR star, the surface magnetic field is of the order of  $B_s = 10^3$  G and the  $v_{\text{rot}} \approx 0.1 R_\infty$ . The Alfvén radius is located then at  $R_A = 1.12 \times R_s$ , and  $R_{\text{tor}} = 10 \times R_s$ . Therefore, the main volume of the MSWR, in which IC  $e^\pm$  pair cascade can efficiently develop, is dominated by the magnetic field with the radial structure.

#### 4.2 Propagation of leptons in MSWR

The equations of motion of a charged particle in a constant uniform magnetic field (see Jackson 1962) are described in the coordinate system in which the vector of the magnetic field,  $\vec{B}$ , is parallel to the axis OZ. Then, the coordinate of the charged particle and its velocity is given by,

$$\vec{r}(t) = \vec{r}_0 + v_{\parallel} t \vec{e}_3 + a \cos \omega_B t \vec{e}_2 + a \sin \omega_B t \vec{e}_1, \quad (18)$$

$$\vec{v}(t) = v_{\parallel} t \vec{e}_3 + \omega_B a (\cos \omega_B t \vec{e}_1 + \sin \omega_B t \vec{e}_2), \quad (19)$$

where  $\vec{e}_3$  is a unit vector parallel to the magnetic field line,  $\vec{e}_1$  and  $\vec{e}_2$  are the other orthogonal unit vectors,  $\omega_B = e\vec{B}/\gamma mc = ec\vec{B}/E$  is the Larmor frequency and  $\omega_B a = v_{\perp}$  is the perpendicular velocity of the charged particle with respect to the magnetic field line while  $v_{\parallel}$  denotes component along the field, and  $a$  is the Larmor radius. Using these equations we follow the charged particle by determining its position and velocity vector with respect to the local magnetic field line.

The step distance method is applied to follow the path of the particle in the magnetic field. The dimension of the step is chosen to be less than 0.01 of the Larmor radius in the local magnetic field. The optical depth for lepton on

the IC scattering is calculated by summing up contributions from every step up to the moment of fulfilling the condition for simulating the place of interaction (given by Eq. 9). Note that this procedure is much more complicated and time consuming than applied in the PWZ since now we have to determine the direction of lepton at every step. We calculate the energy of produced secondary  $\gamma$ -ray photons applying the procedure described in Sect. 3.1 (see Eq. 11). The energy of surviving leptons is equal to the difference between its initial energy and the energy of produced  $\gamma$ -ray photons. Therefore, after every scattering the conditions for propagation of leptons in the magnetic field change due to the change of their Larmor radius. The particle paths are followed up to the moment when leptons: (1) are cooled below 500 MeV, (2) move outside the sphere with the radius of 10 massive star radii (since the efficiency of IC scattering at larger distances becomes low), (3) fall onto the massive star surface, or (4) move back through the shock plane. The energies and directions of produced  $\gamma$ -rays are stored and used for analysis of their spectral and angular properties.

#### 4.3 Angular distribution of escaping gamma-rays

Let us investigate the angular distribution of secondary  $\gamma$ -rays produced by secondary  $e^\pm$  pairs which in turn originate in the absorption process of  $\gamma$ -rays from PWZ cascade. These  $e^\pm$  pairs propagate in the magnetic field and anisotropic soft radiation. As before, we consider two cases of the monoenergetic and power law injection of primary leptons. In Figs. 6 and 7 the distribution of secondary  $\gamma$ -rays on the sky are shown in the case of primary leptons injected at specific directions defined by the angles  $\theta = 90^\circ$  (Figs. 6a and 7a),  $120^\circ$  (Figs. 6b and 7b), and  $150^\circ$  (Figs. 6c and 7c). These numbers are shown for one injected monoenergetic lepton with energy  $10^6$  MeV (Fig. 6) and for the power law spectrum of leptons with the power normalized to  $10^6$  MeV (Fig. 7). The  $\gamma$ -rays are sorted by their escape directions, i.e. within the regions on the sky defined by the azimuthal directions ( $\varphi = 180^\circ$  corresponding to the case of the massive star in front of the pulsar) and by the cosine of the vertical angle  $\beta$ . The basic features of the angular distribution of the secondary  $\gamma$ -rays are determined by the structure of the magnetic field in the MSWR. For the parameters considered in this work, the magnetic field is mainly radial in the region above the shock. For the primary leptons injected at the angle  $\theta = 90^\circ$ , the  $\gamma$ -rays from cascade inside the MSWR are mainly produced inside the cone centred along the direction of propagation of  $\gamma$ -rays produced inside the PWZ. Since the magnetic field lines are radial, the angles at which the secondary  $\gamma$ -rays escape are limited to relatively small part of the sphere (see Figs. 6a and 7a). For primary leptons injected at larger angles, see e.g.  $\theta = 120^\circ$  and  $150^\circ$  (Figs. 6bc and 7bc), the cone of secondary  $\gamma$ -ray production inside the MSWR becomes broader on the sky. Most efficient production occurs for directions which are tangent to the massive star limb (see Figs. 6c and 7c for the angle  $\theta = 150^\circ$ ). In this case a significant part of secondary  $\gamma$ -rays fall onto the surface of the massive star which angular dimensions, seen from the location of the neutron star, are equal to  $26.4^\circ$  (note the avoidance region centred on  $\varphi = 180^\circ$  and  $\cos \beta = 0$  in Figs. 6c and 7c). If the primary leptons are injected exactly

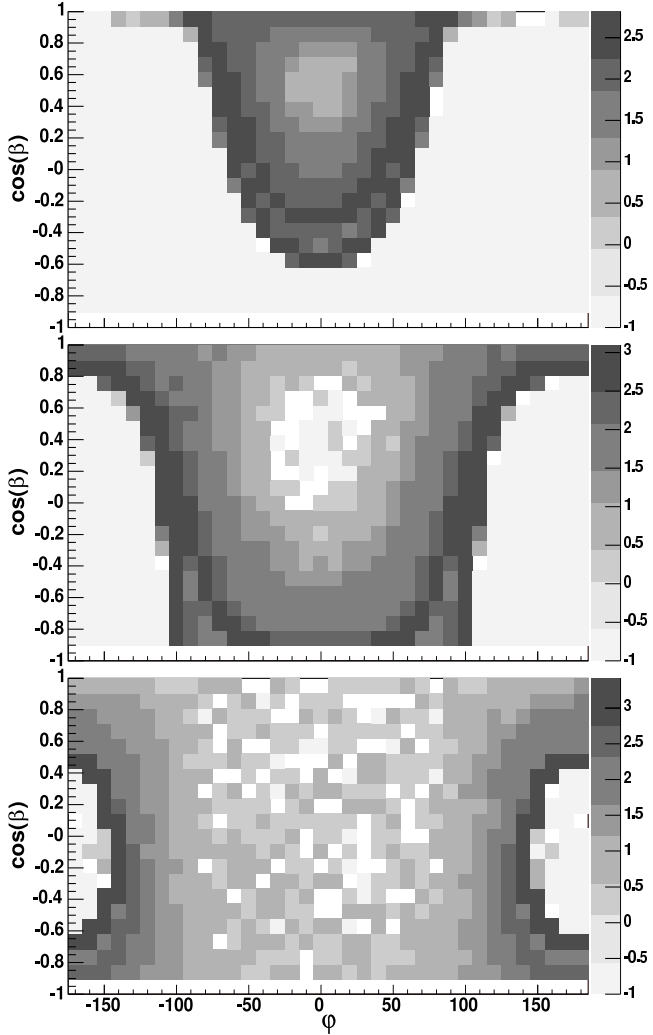


**Figure 6.** The maps with the numbers of  $\gamma$ -ray photons with energies  $> 100$  MeV (in log grey scale) escaping at specific directions on the sky defined by the azimuthal angle  $\varphi$  and the cosine of the vertical angle  $\beta$  (the bins with  $\Delta\varphi = 10^\circ$  and  $\cos \beta = 0.1$ ).  $\varphi = 0^\circ$  correspond to the case of the massive star in front of the pulsar which is the source of primary leptons. These  $\gamma$ -rays are produced in the cascade in the MSWR initiated by the secondary cascade  $\gamma$ -rays escaping from the PWZ, which in turn were produced by primary monoenergetic leptons with energies  $10^6$  MeV. The results, averaged over  $N$  simulated primary leptons, are shown for different initial injection angles of the primary leptons equal to  $\theta = 90^\circ$  for  $N = 200$  (a),  $120^\circ$  for  $N = 100$  (b), and  $150^\circ$  for  $N = 60$  (c), which are measured above the plane of the binary system (i.e. towards positive vertical angles). Presented results are re-normalized for one lepton with energy  $10^6$  MeV.

towards the massive star ( $\theta = 180^\circ$ ), then the secondary  $e^\pm$  leptons, which originate in the MSWR in absorption of secondary  $\gamma$ -rays from PWZ, move along the radial magnetic field. Most of the  $\gamma$ -rays produced in MSWR fall then onto the massive star. The secondary  $e^\pm$  pairs reach finally the dipole part of the magnetic field, which is close to the massive star, and may produce low energy  $\gamma$ -rays at wide angles in the plane of the binary system.

The angular distribution of  $\gamma$ -rays produced in the MSWR in the case of monoenergetic and power law distribu-

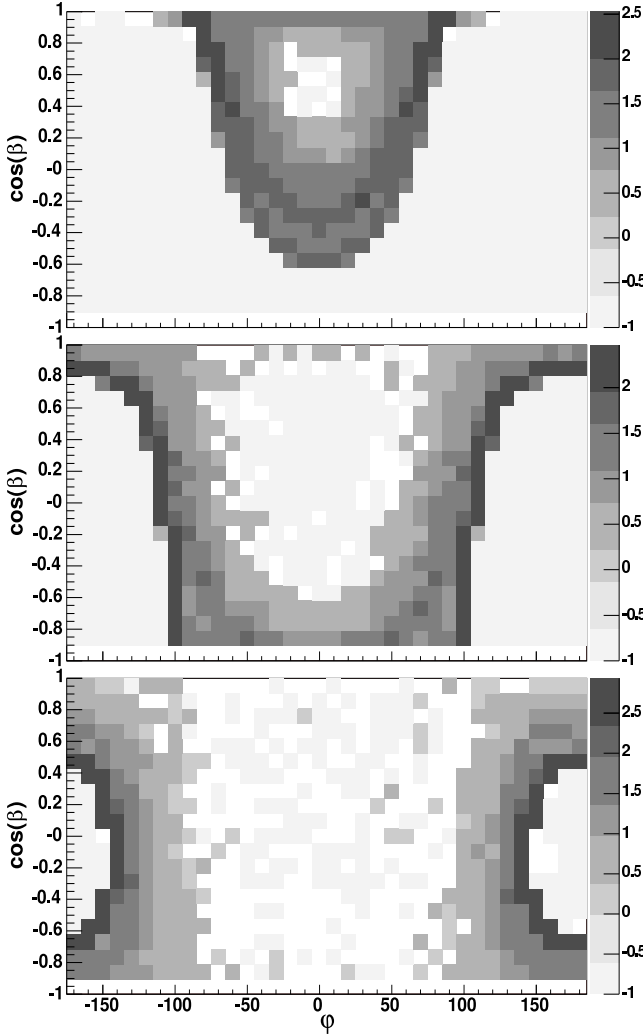


**Figure 7.** As in Fig. (6) but for the primary leptons with the power law spectrum (described in the text) which energy is also normalized to  $10^6$  MeV. The results are averaged over 500 simulated primary leptons for the angle of injection  $\theta = 90^\circ$  (a), 180 leptons for  $120^\circ$  (b), and 150 leptons for  $150^\circ$  (c).

tions of primary leptons is similar since it is determined by the radial structure of the magnetic field. However, the numbers of produced  $\gamma$ -rays are a factor of a few larger in the case of monoenergetic injection of primary leptons. This is due to the fact that  $\gamma$ -rays produced in the PWZ by monoenergetic leptons have on average higher energies (see Figs. 3ac). Therefore they transport more energy to the MSWR. The energies and numbers of secondary  $e^\pm$  pairs, from their absorption inside the MSWR, are larger allowing more efficient production of next generation of  $\gamma$ -rays in the MSWR.

The angular distributions of  $\gamma$ -rays with energies  $> 100$  MeV which escape to the observer from the MSWR for the case of isotropic injection of primary leptons are shown in Fig. 8. The numbers of these  $\gamma$ -rays are normalized to the power in primary lepton spectrum equal to  $10^6$  MeV sr $^{-1}$ . As before, the pulsar is behind the massive star for the phase  $\varphi = 180^\circ$ . As expected, the numbers of produced  $\gamma$ -rays are the largest in directions tangent to the limb of the massive star. Significantly lower numbers of  $\gamma$ -rays emerge from the

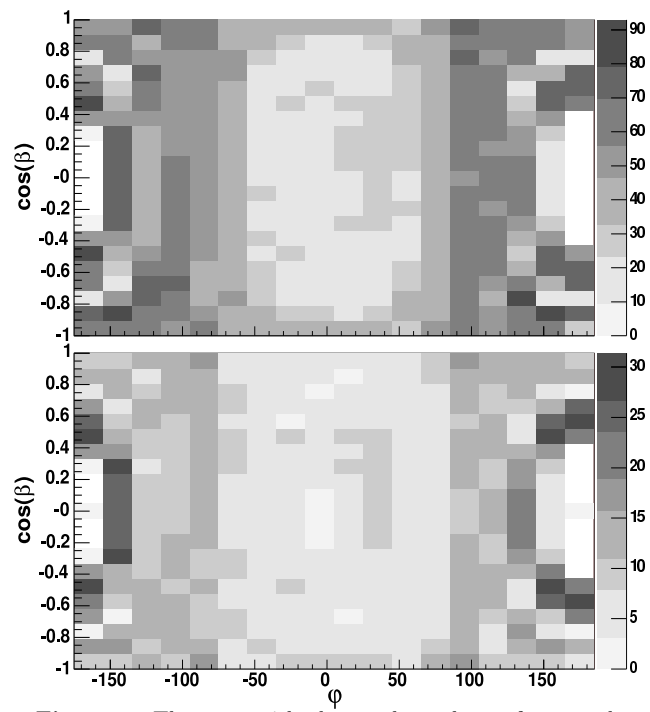


**Figure 8.** The map with the total numbers of  $\gamma$ -ray photons with energies  $> 100$  MeV (in linear grey scale), escaping from the binary at specific directions on the sky (defined by the azimuthal angle  $\varphi$  and cosine of horizontal angle  $\cos \theta$ ) for the case of isotropic injection of primary monoenergetic leptons with energies  $10^6$  MeV (a) and for the primary leptons with the power law spectrum described in the text (b).  $\gamma$ -rays are produced in cascades inside the MSWR initiated by secondary cascade  $\gamma$ -rays from the PWZ. The spectra of primary leptons are normalized to their total energy equal to  $10^6$  MeV per steradian.

binary system in the outward directions, i.e. in directions for which the pulsar is in front of the massive star with respect to the observer. Note that in these directions the MSWR does not extend (see Fig. 1).

#### 4.4 Gamma-ray light curves and spectra

The  $\gamma$ -ray light curves of photons produced in the MSWR (Table 4) for two energy ranges,  $0.1 - 10$  GeV and  $10$  GeV -  $1$  TeV, are shown in Figs. 9, after its normalization to the total energy loss rate of the considered here pulsar. The observer is located at different inclination angles  $i$  to the plane of the binary system. The general features of the  $\gamma$ -ray light curves produced in the MSWR are similar to these ones shown above for the  $\gamma$ -rays produced in the PWZ (see for comparison Figs. 9). However, the total  $\gamma$ -ray power is usually lower (typically by a factor of three) than expected in the case of  $\gamma$ -rays produced in the PWZ. Only in the range of phases around  $0^\circ$ , and large inclination angles, the power of the  $\gamma$ -rays from the MSWR can dominate over the PWZ  $\gamma$ -rays in the GeV energy range.

The power emitted in GeV energies is quite uniform with the phase of the pulsar provided that the inclination angle is small enough that the binary system is not eclipsing. The power emitted at TeV energies is limited to the range of

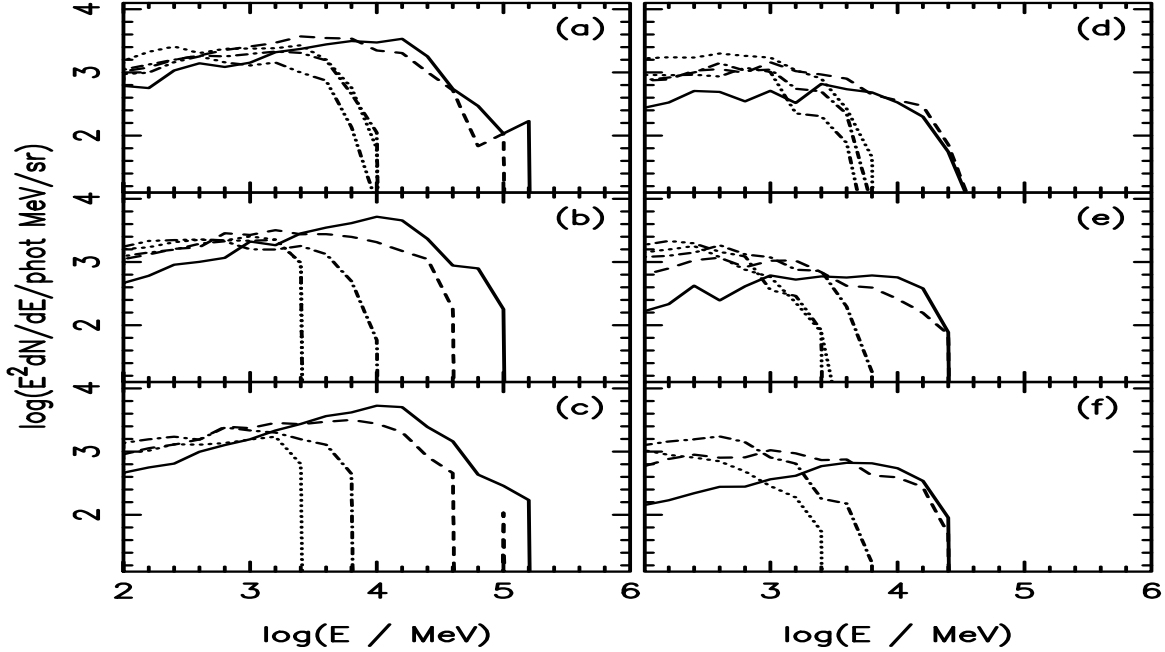


**Figure 10.** The  $\gamma$ -ray spectra escaping from the MSWR for different phases of the pulsar with respect to the location of the observer,  $\varphi = 30^\circ$  (solid curve)  $60^\circ$  (dashed),  $90^\circ$  (dot-dashed),  $120^\circ$  (dotted),  $180^\circ$  (dot-dot-dot-dashed), and three ranges of the cosine of the inclination angle of the binary  $0.76 < \cos \alpha < 0.88$  (centered on  $i = 30^\circ$  - (a) and (d)),  $0.41 < \cos \alpha < 0.53$  ( $60^\circ$  - (b) and (e)), and  $-0.06 < \cos \alpha < 0.06$  ( $90^\circ$  - (c) and (f)).  $\gamma$ -rays are produced in the MSWR cascade by secondary  $e^\pm$  pairs which in turn originate in the absorption of  $\gamma$ -rays produced in the PWZ by primary leptons with the monoenergetic (figures on the left) and power law spectrum (on the right).

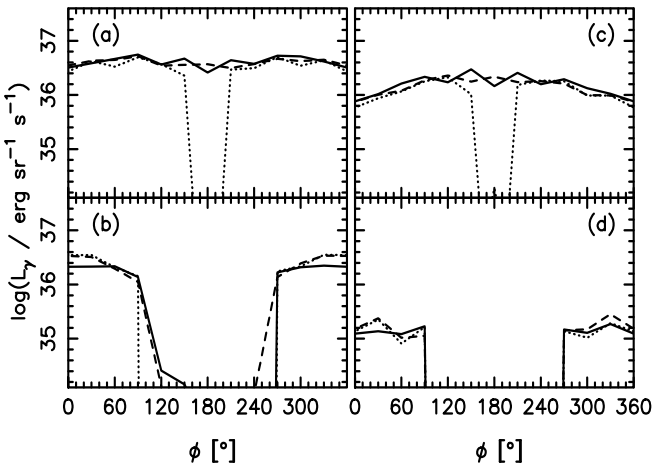


**Figure 9.** The  $\gamma$ -ray light curves in two energy ranges,  $0.1 - 10$  GeV ((a) and (c)) and  $10 - 10^3$  GeV ((b) and (d)), produced in the MSWR cascade initiated by secondary  $\gamma$ -rays which are in turn produced in the cascade in the PWZ initiated by primary leptons with the monoenergetic (figures on the left) and the power law distributions (on the right).  $\gamma$ -rays escaping from the MSWR are collected within the range of the cosine of inclination angles of the system  $0.76 < \cos i < 0.88$  (contains  $i = 30^\circ$  - solid curve),  $0.41 < \cos i < 0.53$  ( $60^\circ$  - dashed), and  $-0.06 < \cos i < 0.06$  ( $90^\circ$  - dotted).

phases  $\pm 60^\circ$  around the phase  $0^\circ$  which correspond to the position of the pulsar in front of the massive star.

Figs. 10 show the  $\gamma$ -ray spectra produced in the MSWR for selected phases and inclination angles of the binary system. The basic differences between these spectra and the

$\gamma$ -ray spectra produced in the PWZ are due to the fact that cascade in the MSWR is initiated by leptons for which the total optical depths are higher. Therefore, these  $\gamma$ -ray spectra are steeper, with the spectral index close to -2, in contrast to the spectral index of the spectra produced in the PWZ which are close to -1.5. Although, the power emitted in  $\gamma$ -rays from the MSWR is a factor of a few lower. It can still significantly contribute to the total  $\gamma$ -ray spectrum observed at some range of phases and at energies below  $\sim 1$  GeV for the case of monoenergetic injection of primary leptons. Moreover, as already noted above, this GeV emission is much more uniform over the sky. At energies  $> 10$  GeV the contribution of the  $\gamma$ -rays from the MSWR (produced by monoenergetic primary leptons) becomes negligible with respect to the  $\gamma$ -rays from the PWZ for the considered location of the shock inside the binary system defined by  $\eta = 0.3$ . The  $\gamma$ -rays produced inside the MSWR by primary leptons with the power law spectrum (see Figs. 10def) do not contribute significantly to the  $\gamma$ -rays produced in the PWZ (Figs. 5def). Primary leptons with the power law spectrum produce on average more secondary  $\gamma$ -rays already inside the PWZ.

## 5 DEPENDENCE ON THE SHOCK LOCALIZATION

Since detailed parameters of the massive stellar winds are not precisely known we investigate the dependence of escaping  $\gamma$ -ray spectra on the location of the shock inside the binary system by performing calculations for the same initial injection spectra of leptons but for the shock determined by the value of  $\eta = 0.06$ . This value is obtained for upper limits

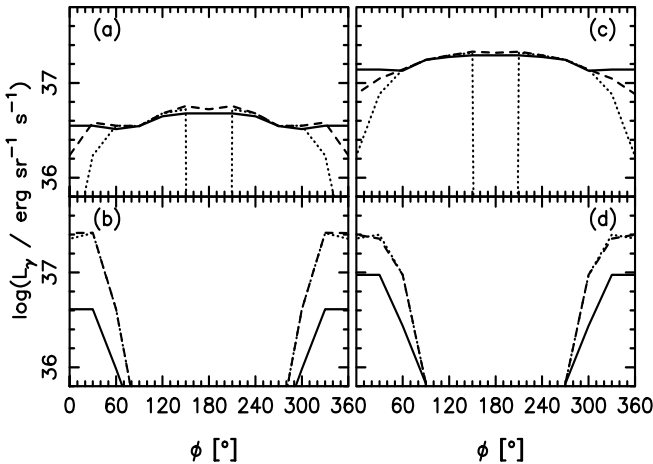


Figure 11. As in Fig. 4 but for  $\eta = 0.06$ .

of the stellar wind parameters (see Sect. 2). For  $\eta = 0.06$  the shock is located at the distance of  $\rho_0 = 0.25 R_s$  from the pulsar, i.e. about two times closer than for  $\eta = 0.3$ , and the volume for the development of the cascade in the PWZ is much smaller than for the cascade in the MSWR.

### 5.1 Gamma-rays from PWZ

For leptons injected with the power law spectrum, the  $\gamma$ -ray luminosities produced in the PWZ (and detected by the observer at the infinity) for  $\eta = 0.06$  are only slightly lower than for  $\eta = 0.3$  (see for comparison the  $\gamma$ -ray light curves and spectra in Figs. 11 and 12 with Figs. 4 and 5, respectively). This small differences are not surprising since the energy from primary leptons with the power law spectrum is transferred to  $\gamma$ -rays efficiently already inside the PWZ due to large optical depths for leptons with energies much lower than  $10^6$  MeV (see Fig. 2). However, the reduction of  $\gamma$ -ray fluxes is much stronger for leptons injected with the monoenergetic spectrum and energies  $10^6$  MeV. The  $\gamma$ -ray light curves and spectra for the monoenergetic primary leptons and the shock defined by  $\eta = 0.06$  are by a factor of about 3 lower than for  $\eta = 0.3$ . As shown in Fig. 2c, the optical depths for leptons with energies  $10^6$  MeV are close to unity for  $\eta = 0.06$  but much larger for  $\eta = 0.3$ . Therefore, the differences in the cascades developed in the PWZ by high energy monoenergetic leptons are larger than reported for leptons with the power law spectrum.

Large differences between these two discussed localizations of the shock in the  $\gamma$ -ray light curves in the energy range  $10 - 10^3$  GeV are also observed for small inclination angles  $i$  (see Figs. 4b and 11b). They are due to lower optical depths for monoenergetic leptons with energies  $10^6$  MeV. Leptons injected in directions perpendicular to the plane of the binary system meet on its propagation through the PWZ smaller number of soft photons from the massive companion than these ones propagating towards the massive star due to the geometrical effects. Moreover, the spectra of  $\gamma$ -rays escaping to the infinity for  $\eta = 0.06$  show cut-offs at lower energies than in the case of the shock defined by  $\eta = 0.3$ . This effect, especially clear for the monoenergetic injection of primary leptons, is due to the stronger absorption of higher

energy  $\gamma$ -rays during their propagation in the MSWR which volume is larger for  $\eta = 0.06$  than for  $\eta = 0.3$ .

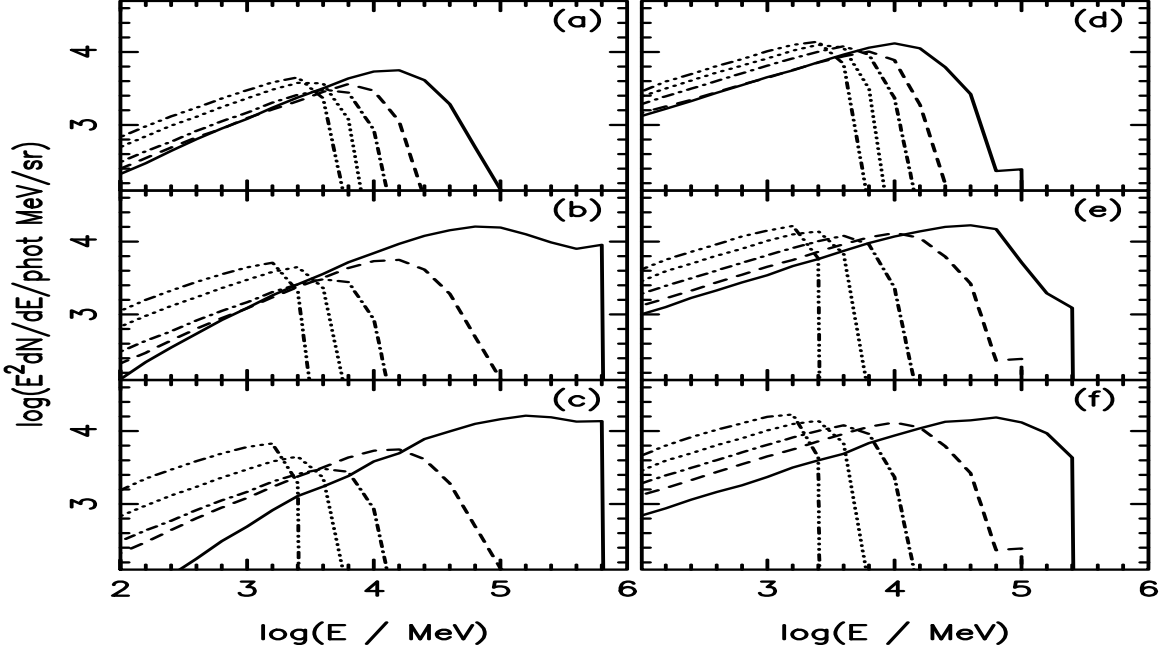
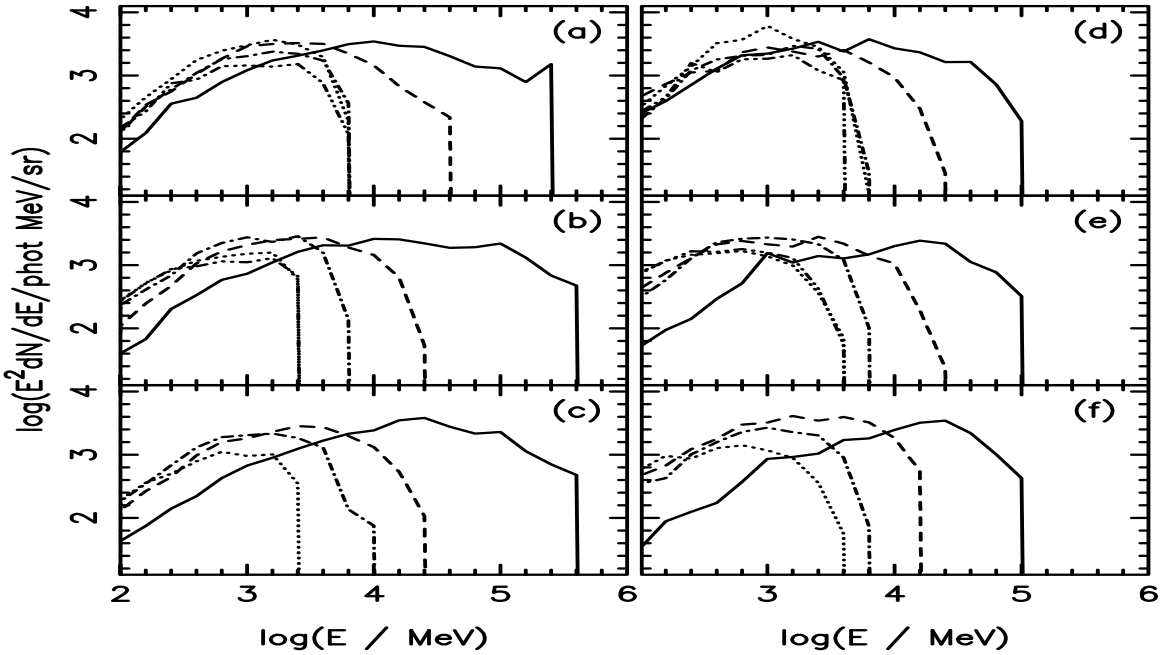
### 5.2 Gamma-rays from MSWR

Basic differences in the  $\gamma$ -ray production in the MSWR due to different localizations of the shock inside the massive binary (defined by  $\eta = 0.3$  and  $0.06$ ) are related to the efficiency of the cascades occurring already inside the PWZ since  $e^\pm$  pairs, created in absorption of the PWZ  $\gamma$ -rays, are responsible for production of  $\gamma$ -rays in the MSWR. For localization of the shock described by  $\eta = 0.06$ , the  $\gamma$ -ray spectra produced in the MSWR extend to higher energies than for the case of  $\eta = 0.3$  (see Figs. 10 and 14). This is also clearly seen when investigating the  $\gamma$ -ray light curves at energies  $> 10$  GeV for the case of the power law spectrum of primary leptons shown in Figs. 9d and 13d. This behavior is in contrast to the features of the  $\gamma$ -ray spectra produced in the PWZ. It is clear from the Table 1b that, although the  $\gamma$ -ray luminosity leaving the PWZ (i.e. entering the MSWR) for the power law spectra of primary leptons is comparable for  $\eta = 0.3$  and  $0.06$  (see percentages marked by *shock*), the power transformed to the secondary  $e^\pm$  pairs in the MSWR, from absorption of the PWZ  $\gamma$ -rays, differ significantly due to much larger volume of the MSWR for  $\eta = 0.06$  (see differences between percentages marked by *shock* and *esc*). Therefore, secondary  $e^\pm$  pairs produced in the MSWR for the shock located closer to the pulsar (i.e. for  $\eta = 0.06$ ) have, on average, higher energies and produce more energetic  $\gamma$ -rays in the MSWR. This is also the reason that the  $\gamma$ -ray light curves are on a slightly higher level for  $\eta = 0.06$  (compare Figs. 9cd with 13cd).

For the case of the monoenergetic injection of primary leptons, the  $\gamma$ -ray luminosity originating in the PWZ is clearly lower for  $\eta = 0.06$  (Table 1a). However, the energy transferred into the secondary  $e^\pm$  pairs in the MSWR, as a result of absorption of the PWZ  $\gamma$ -rays, is comparable for both of the shock localizations (note differences between percentages marked by *shock* and *esc* in Table 1a). Therefore, differences in the  $\gamma$ -ray light curves and spectra for the localizations of the shock inside the binary system defined by  $\eta = 0.3$  and  $0.06$  are not so evident than in the case of the power law injection of primary leptons.

## 6 DISCUSSION AND CONCLUSIONS

We have analyzed in details the anisotropic IC  $e^\pm$  cascade inside the massive binary system containing young pulsar. We have considered the situation in which leptons are injected mono-directionally or isotropically from a place (identified with the pulsar) which differs from the center of the isotropic source of soft radiation (identified with the massive stellar companion). The simplest geometrical situation has been analyzed in which a compact object is on a circular orbit around the massive star. As an example, the parameters of the massive binary in the Cyg X-3 system have been applied. We concentrate on the situation in which a pulsar is energetic enough to create strong shock in collision with the wind of the massive star. As a consequence, two regions for the development of the cascade has to be distinguished which differ in basic properties, i.e. the pulsar wind zone (PWZ)

Figure 12. As in Fig. 5 but for  $\eta = 0.06$ .Figure 14. As in Fig. 7 but for  $\eta = 0.06$ .

and the massive star wind region (MSWR). In the PWZ the cascade develops radially from the pulsar and therefore can be considered only in one direction. In the MSWR the cascade develops in complex magnetic field of the massive star. Therefore, complicated propagation paths of secondary  $e^\pm$  pairs in this magnetic field have to be taken into account. However, for typical values of the magnetic fields in the winds of the massive stars and parameters of Cyg X-3 binary, the energy density of radiation from the massive star is larger than the energy density of the magnetic field. Hence, the IC energy losses of leptons dominate over their synchrotron losses and the influence of synchrotron process

on the energy budget of leptons can be neglected in the first approximation.

For this specific binary system we have calculated the optical depths for leptons and  $\gamma$ -rays and found that they are much larger than unity (Fig. 2). Therefore, if relativistic leptons are injected inside the binary they should initiate efficient cascades. Such cascades are analyzed in the case of leptons injected by the compact object with: (a) the monoenergetic spectrum and energies  $10^6$  MeV and, (b) the power law spectrum of the type predicted by the calculations of the cascade processes in the inner pulsar magnetosphere (Hirschman & Arons 2001).

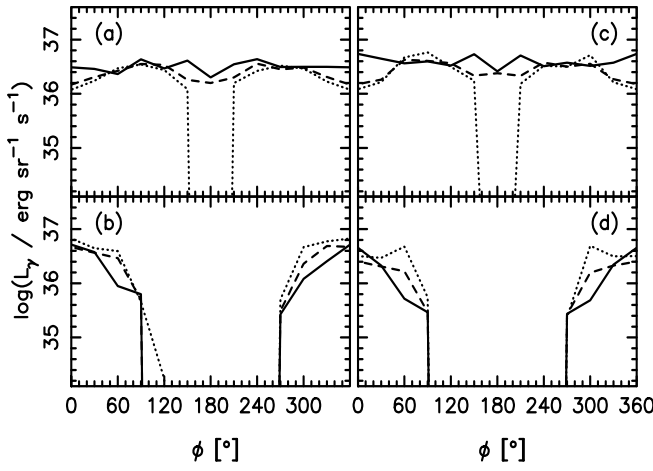


Figure 13. As in Fig. 6 but for  $\eta = 0.06$ .

The main results of our calculations are following:

(i) Most of the energy of primary leptons is transferred to the secondary  $\gamma$ -rays ( $\sim 80 - 90\%$ , see Table 1) for both the monoenergetic and the power law primary spectra, and for the shock defined by  $\eta = 0.3$  which correspond to the case of the massive star with the wind parameters from the middle of the estimated range (Sect. 2). This percentage of energy does not depend strongly on the location of the shock for the power law spectrum of primary leptons (compare  $\eta = 0.3$  and 0.06 in Table 1), but is significantly lower for the shock closer to the pulsar, determined by  $\eta = 0.06$  in the case of monoenergetic primary leptons. The difference between the power in  $\gamma$ -rays arriving to the shock (marked by *shock*) and  $\gamma$ -rays escaping to the observer (marked by *esc*) gives part of the power of  $\gamma$ -rays produced in the PWZ which is converted into the secondary  $e^\pm$  pairs in the MSWR. These  $e^\pm$  pairs can initiate additional cascade in the MSWR and take typically between one third and half of the  $\gamma$ -ray power escaping to the observer from the PWZ (see Table 1). Therefore, the contribution of  $\gamma$ -rays produced in the MSWR is usually lower than  $\gamma$ -rays produced in the PWZ. However, if the monoenergetic primary leptons are injected into the binary with the shock located relatively close to the pulsar (e.g. for  $\eta = 0.06$ ) the  $\gamma$ -ray luminosity produced in the MSWR can be even a factor of two or three larger than  $\gamma$ -ray luminosity from the PWZ. This is due to lower optical depths in relatively small PWZ and so inefficient cascading precess initiated by high energy monoenergetic leptons.

(ii) The  $\gamma$ -ray light curves for photons escaping from the PWZ at lower energies (energy range  $0.1 - 10$  GeV) are anticorrelated with the  $\gamma$ -ray light curves at higher energies ( $> 10$  GeV) for both discussed primary spectra of leptons independently on localizations of the shock within the binary system (see e.g. the  $\gamma$ -ray light curves in Figs. 4 and 11). This basic feature is also clearly seen when comparing the  $\gamma$  spectra escaping to the observer at different phases of the pulsar and inclinations of the binary system (Figs. 5 and 12). It is easily understood since the intense  $\gamma$ -ray fluxes at energy range  $0.1 - 10$  GeV are expected in directions of large optical depths, when the binary system is viewed from the direction close to the massive star. In contrast, high level  $\gamma$ -ray fluxes at energies  $> 10$  GeV are expected when the

compact object is in front of the massive star. For considered parameters of the binary system, the optical depth is high enough for efficient production of  $\gamma$ -rays above 10 GeV but is too low for efficient cascading and production of lower energy  $\gamma$ -rays. Moreover, the  $\gamma$ -ray spectra extend to higher energies for the monoenergetic primary leptons but are less intense at lower energies than expected for the power law primary leptons (see Figs. 5 and 12) since the optical depths are lower for higher energy particles (see Figs. 2). Therefore, it is expected that detailed results in the  $\gamma$ -ray spectra from specific binaries (PSR B1259-63, SAX J 0635+0533), for which the parameters of the massive star are well known, should allow to obtain information on the spectrum of primary leptons accelerated by the pulsar. This problem is difficult to investigate directly in the case of isolated pulsars for which the surrounding soft radiation field in the pulsar wind zone is relatively weak.

(iii) The complex magnetic field in the MSWR has significant effect on the directions of propagation of secondary  $e^\pm$  pairs and, as a consequence, on the distribution of  $\gamma$ -rays on the sky. Our detailed calculations show that the angular distribution of  $\gamma$ -rays, produced in the cascade processes in the MSWR by secondary  $e^\pm$  pairs from absorption of  $\gamma$ -rays from PWZ, strongly depends on the injection direction of primary leptons (see maps in Figs. 6 and 7). For example, if the primary particles are injected perpendicular to the plane of the binary system then the  $\gamma$ -rays produced in the cascade are collimated within the cone around the direction of the local magnetic field lines, i.e. in the outward direction with respect to the massive star (Figs. 6a and 7a). This is due to the strong radial component of the massive star magnetic field in the main volume of the binary system (see Eq. 11). Therefore, in the case of highly anisotropic injection of primary particles by the pulsar, the strong  $\gamma$ -rays fluxes may appear in quite different directions. In contrast, if the primary particles are injected in the directions not far from the stellar limb, this radial component of the magnetic field tends to focus the  $\gamma$ -rays in directions tangent to the stellar limb. A significant part of these  $\gamma$ -rays impinge onto the surface of the massive star (see Figs. 6c and 7c). It is expected that these  $\gamma$ -rays can excite observable nuclear  $\gamma$ -ray line fluxes due to their interactions with the matter on the massive star surface. This line emission should be correlated with the high energy  $\gamma$ -ray emission ( $> 10$  GeV) and anticorrelated with the low energy  $\gamma$ -ray emission (between  $0.1 - 10$  GeV).

The distribution of  $\gamma$ -rays produced in the MSWR is also strongly anisotropic for the case of isotropic injection of primary leptons by the pulsar (see Fig. 8). There is a strong concentration of produced secondary  $\gamma$ -rays in directions close to the limb of the massive star. The number of secondary photons produced by the primary leptons with the power law spectrum is by a factor of a few lower than for monoenergetic primary leptons but general emission pattern on the sky does not differ significantly. These features are due to the fact that leptons with lower energies produce  $\gamma$ -rays with energies above 100 MeV less efficiently.

(iv) The  $\gamma$ -ray fluxes produced in the MSWR are weakly dependent on the phase of the pulsar and the inclination angles of the binary system, except for the case of eclipsing binaries (see Figs. 9 and 13). This is due to the propagation effects of secondary  $e^\pm$  pairs in the magnetic field

of the MSWR which result in a significant isotropisation of the secondary  $e^\pm$  pairs with respect to the directions of propagation of primary leptons. Therefore, when the pulsar is in front of the massive star (phase  $\varphi = 0^\circ$ ), the main contribution to the escaping low energy  $\gamma$ -ray flux comes from the MSWR and the anticorrelation between the lower energy ( $0.1 - 10$  GeV) and higher energy ( $> 10$  GeV)  $\gamma$ -rays produced in the PWZ is partially suppressed (compare Figs. 4 with 9 and 11 with 13). The  $\gamma$ -ray spectra escaping to the observer from the MSWR are flatter in the GeV energy range (spectral index close to -2) than the  $\gamma$ -ray spectra from the PWZ (spectral index close to -1.5) (compare Figs. 5 with 10 and 12 with 14). This is due to the difference in the optical depth for particles propagating in the PWZ and the MSWR. Since the cascade is not efficient enough in the PWZ, the secondary  $e^\pm$  pairs are not able to influence lower energy part of the IC  $\gamma$ -ray spectrum formed mainly by cooling of primary leptons. However, secondary  $e^\pm$  pairs in the MSWR are cooled to energies low enough to produce a lot of secondary GeV photons and thus creating steeper spectra. Due to the same reasons, the  $\gamma$ -ray spectra from the MSWR extend usually to lower energies and the predicted fluxes above  $\sim 10$  GeV are lower.

(v) The  $\gamma$ -ray spectra escaping from the MSWR depend strongly also on the localization of the shock inside the binary. This is caused by the change in relative volume for the development of cascades in the PWZ and MSWR. If the shock is closer to the pulsar then the  $\gamma$ -ray spectra from the MSWR extend to higher energies (see Figs. 10 and 14) since they are produced by on average more energetic secondary  $e^\pm$  pairs originated in the absorption of more energetic  $\gamma$ -rays escaping from the PWZ. The  $\gamma$ -ray fluxes at energies  $< 10$  GeV, produced in the MSWR, do not depend strongly on the localization of the shock. But the  $\gamma$ -ray fluxes at energies  $> 10$  GeV are on a much lower level for the case of primary leptons injected with the power law spectrum (see Figs. 9 and 13) from the same reasons as discussed in this item above.

In summary, detailed investigation of the phase resolved IC continuous  $\gamma$ -ray spectra and the  $\gamma$ -ray light curves from the compact massive binaries, in which energetic pulsar is responsible for the acceleration of relativistic leptons, should allow extraction of information on the primary spectra of leptons (monoenergetic, power law ?) and conditions for collisions of the pulsar and stellar winds. The fluxes and spectra of escaping  $\gamma$ -rays should be also sensitive to the acceleration site of the primary leptons, inside the inner pulsar magnetosphere (power law spectrum ?), close to the pulsar light cylinder (monoenergetic ?), or during the propagation in the pulsar wind zone (see e.g. re-acceleration model of Contopoulos & Kazanas 2002). The effects on the  $\gamma$ -ray spectra caused by leptons which are additionally accelerated in the pulsar wind zone have been recently investigated with the application to the PSR B1259-63/Be binary system (Sierpowska & Bednarek 2004b), but they need further more detailed calculations.

Taking into account sensitivities of the future and already operating  $\gamma$ -ray telescopes in the energy range below a few hundred GeV (which are estimated on  $\sim 3 \times 10^{-13}$  erg  $\text{cm}^{-2} \text{s}^{-1}$  for the GLAST and  $\sim 10^{-12}$  erg  $\text{cm}^{-2} \text{s}^{-1}$  for the MAGIC), the type of the massive binary considered in this

paper with the  $\gamma$ -ray luminosity of the order of  $\sim 10^{37}$  erg  $\text{sr}^{-1} \text{s}^{-1}$  (similar to the Cyg X-3 massive binary) should be detected at any location within our Galaxy and also within the Magellanic Clouds.

In the forthcoming paper (Sierpowska & Bednarek 2004a) we intend to apply such general model for the  $\gamma$ -ray production in specific massive binaries in which case there are evidences of the existence of energetic pulsars (e.g. PSR B1259-63, SAX J0635) or compact objects with jets (see the list of sources in Table 1 in Mirabel & Rodriguez 1999). Note that in the case of less compact binaries than considered here, the secondary cascade  $e^\pm$  pairs arrive to the shock with significant energies since the optical depths for leptons are much lower. These pairs move then along the shock plane. Their contribution to the total escaping  $\gamma$ -ray fluxes has to be also taken into account. It has not been considered in this paper since, for the parameters of the massive star in the Cyg X-3, these pairs take only a relatively small part of energy of primary leptons (typically less than  $\sim 20\%$  of the total injected energy, see Table 1). Therefore, relative importance of processes occurring in the PWZ, the shock region, and the MSWR can differ significantly for the very close binaries with the pulsars on circular orbits (as considered here) from the binaries of the PSR 1259-63 type, i.e. with a broad, highly eccentric orbit and a massive Be star producing non-spherical stellar wind.

We also plan to investigate possible importance of the cascade processes inside the binary systems of two very massive stars which create strong shock as a result of their stellar wind collisions, e.g.  $\gamma$ -2 Vel (WC8+O7.5). Energetic  $e^\pm$  pairs can appear inside such binaries as a result of interaction of hadrons, accelerated by the shock, with radiation field of the massive star.

## ACKNOWLEDGMENTS

We thank the referee, Dr G.E. Romero, for many useful comments and suggestions. This work is supported by the Polish KBN grants No. 5P03D02521 and PBZ KBN 054/P03/2001.

## REFERENCES

- Aharonian, F. A., Atoyan, A.M. 1991, *ApJ* 381, 220
- Aharonian, F. A., Atoyan, A.M. 1999, *MNRAS*, 302, 253
- Atoyan, A.M., Aye, K.-M., Chadwick, P.M. et al. 2002, *A&A* 383, 864
- Arons, J., Scharlemann, E.T. 1979, *ApJ* 231, 854
- Arons, 1983, *ApJ* 266, 215
- Ball, L., Dodd, J. 2001, *Publ. Astron. Soc. Aust.* 18, 98
- Ball, L., Kirk, J.G. 2000, *APh* 12, 335
- Bednarek, W. 1993, *A&A* 278, 307
- Bednarek, W. 1997, *A&A* 322, 523
- Bednarek, W. 2000, *A&A* 362, 646
- Bednarek, W., Giovannelli, F., Karakuła, S., Tkaczyk, W. 1990, *A&A* 236, 175
- Benaglia, P., Romero, G.E. 2003, *A&A* 399, 1121
- Beskin, V.S., Rafikov, R.R. 2000, *MNRAS* 313, 433
- Bogovalov, S.V., Aharonian, F.A. 2000, *MNRAS*, 313, 504
- Bosch-Ramon, V., Paredes, J.M. 2004a, *A&A* 417, 1075
- Bosch-Ramon, V., Paredes, J.M. 2004b, in press
- Brazier, A., et al. 1990, *ApJ* 350, 745

Chadwick, P.M., Dickinson, M.R., Dipper, N.A. et al. 1998, ApJ 503, 391

Chadwick, P.M., Lyons, K., McComb, T.J.L. et al. 1999, ApJ 513, 161

Carraminana, A. 1992, A&A 264, 127

Cheng, K.S., Ho, C., Ruderman, M. 1986, ApJ 300, 500

Cheng, K.S., Ruderman, M. 1991, ApJ 373, 187

Cherepashchuk, A., Moffat, A. 1994, ApJ 424, 53

Contopoulos, I., Kazanas, D. 2002, ApJ 566, 336

Daugherty, J.K., Harding, A.K. 1982, ApJ 252, 337

Eichler, D., Usov, V. 1993, ApJ 402, 271

Georganopoulos, M., Aharonian, F.A., Kirk, J.G. 2002, A&A 388, L25

Girard, T., Wilson, L.A. 1987, A&A 183, 247

Hall, T.A., Bond, I.H., Bradbury, S.M. et al. 2003, ApJ 583, 853

Hamann, W.R. 1985, A&A 145, 443

Hanson, M., Still, M., Fender, R. 2000, ApJ 541, 308

Harding, A.K., Gaisser, T.K. 1990, ApJ 358, 561

Hibschman, J.A., Arons, J. 2001, ApJ 560, 871

Jackson, J.D. 1962, *Classical Electrodynamics*, John Wiley & Sons, New York

Kawachi, A., Naito, T., Patterson, J.R. et al. 2004, ApJ 607, 949

Kennel, C.F., Coroniti, F.V. 1984, ApJ 283, 710

Kirk, J.G., Ball, L., Skjæraasen, O. 1999, Astro.Part.Phys 10, 31

Levinson, A., Blandford, R. 1996, ApJ 456, L29

Lipunov, V.M. 1990, *Astrophysics of Neutron Stars*, Springer-Verlag (Berlin)

Maraschi, L., Treves, A. 1981, MNRAS 194, 1

Melatos, A., Johnston, S., Melrose, D.B. 1995, MNRAS 275, 381

Mirabel, I.F., Rodriguez, L.F. 1999, ARAA 37, 409

Mori, M., Bertsch, D.L., Dingus, B.L. et al. 1997, ApJ 476, 842

Moskalenko, I., Karakula, S., Tkaczyk, W. 1993, MNRAS 260, 681

Murata, K., Tamaki, H., Maki, H., Shibasaki, N. 2003, PASJ 55, 467

Nomoto, K., Tsuruta, S. 1987, ApJ 312, 711

Orellana, M., Romero, G.E. 2004, in Proc. The multiwavelength approach to unidentified gamma-ray sources", Eds. K. S. Cheng & G.E. Romero, Kluwer Academic Publisher (Astrophysics and Space Sciences Journal), in press

Paredes, J.M., Marti, J., Ribo, M., Massi, M. 2000, Science 288, 2340

Protheroe, R.J., Stanev, T. 1987, ApJ 322, 838

Romero, G.E., Kaufman Bernado, M.M., Combi, J.A., Torres, D.F., 2001, A&A 376, 599

Romero, G.E., Kaufman Bernado, M.M., Mirabel, I.F. 2002, A&A 393, 61

Romero, G.E., Torres, D.F., Kaufman Bernado, M.M., Mirabel, I.F. 2003, A&A 410, L1

Ruderman, M.A., Sutherland, P.G. 1975, ApJ 196, 51

Schlenker, S. for the HESS collab. 2004, in Proc. Int.Symp.High Energy Gamma-Ray Astronomy (Heidelberg, Germany), AIP, submitted

Sierpowska, A. 2004, PhD thesis, in preparation

Sierpowska, A., Bednarek, W. 2004a, in preparation

Sierpowska, A., Bednarek, W. 2004b, in Proc. International School of Cosmic Ray Astrophysics - 13th Course, eds. M.M. Shapiro, T. Stanev & J.P. Wefel (World Scientific), p.95

Stark, M., Saia, M. 2003, ApJ 587, L101

Tavani, M., Arons, A., Kaspi, V.M. 1994, ApJ 433, L37

Tavani, M., Arons, J. 1997, ApJ 477, 439

Thompson, D.J., Bertsch, D.L., Dingus, B.L. et al. 1995, ApJS 101, 259

Usov, V.V., Melrose, D.B. 1992, ApJ 395, 575

van Kerkwijk, M.H., Geballe, T.R., King, D.L. et al. 2002, A&A 314, 521

Vestrand, W., Eichler, D. 1982, ApJ 261, 251

Vestrand, W.T., Sreekumar, P., Mori, M. 1997, ApJ 483, L49

Weekes, T.C. 1992, Sp.Sci.Rev. 59, 314